Available online at www.sciencedirect.com
SCIENCE DIRECT
Journal of Sound and Vibration 296 (2006) 292–318
JOURNAL OF SOUND AND VIBRATION
www.elsevier.com/locate/jsvi

Linearly coupled shaft-torsional and blade-bending vibrations in multi-stage rotor-blade systems

Özgür Turhan*, Gökhan Bulut

Faculty of Mechanical Engineering, Istanbul Technical University, Gümüşsuyu 34437, Istanbul, Turkey

Received 16 September 2004; received in revised form 20 February 2006; accepted 6 March 2006
Available online 24 May 2006

Abstract

In an attempt towards the understanding of coupling effects between shaft-torsional and blade-(in plane) bending vibrations in turbomachinery and other rotating bladed structures, an idealized model is considered where the blades are represented by uniform Euler–Bernouilli beams. A synthetical, multi-frame and mixed (consisting in a coalescence of finite element and Galerkin methods) approach is used to derive a linearized mathematical model for the system. It is shown that the related eigenanalysis problem splits into two separate sub-problems corresponding to two kinds of possible normal mode motions. Eigenanalyses are performed concerning single as well as multi-stage rotor-blade system examples. Parametric studies are presented on the variation of the eigenfrequencies with system parameters. Eigenvalue loci veering phenomena are shown to occur, causing departure of the eigenvalues from those obtained through an uncoupled analysis. Mode shape examples are also presented.

1. Introduction

Accurate prediction of vibration characteristics is crucial in the design stage of turbomachinery because prototyping and testing costs are exceptionally high and failure is generally disastrous in the practical applications of these systems. As the vibratory failures generally occur in the blades, the researches are mostly focused on the blade vibrations. A review of the theoretical and practical aspects of the problem as well as a literature survey on modelling and analysis of turbomachinery blading was given by Srinivasan [1]. Guided by the pressing needs of the production, the related studies are generally based on a geometrically accurate modelling of the actual systems. Most of the studies feature, therefore, a sophisticated finite element modelling of the blades, blade-carrying disks and other components such as shroudings. Some examples are the works of Ewins [2], Bladh et al. [3] and Tsai [4].

Along with those of the blades, the vibrations of the shaft, especially its bending and torsional vibrations, also deserve a special attention for either their own importance as other major sources of vibratory failures, and their possible coupling with the blade vibrations. However, as the dimension of a finite element model of such a complex structure as a whole turbine is prohibitive unless efficient model reduction techniques are introduced, the classical approach has been to treat the vibrations of the shaft and those of the blading

*Corresponding author.
E-mail address: turhanoz@itu.edu.tr (Ö. Turhan).

0022-460X/$ - see front matter © 2006 Elsevier Ltd. All rights reserved.
doi:10.1016/j.jsv.2006.03.010

separately through uncoupled models, though, in fact, the few works considering the coupling effects pointed to serious interaction between shaft and blade vibrations. In a group of such works Loewy and Khader [5], Crawley et al. [6] and Chun and Lee [7] treated the rotor dynamics problem by considering the coupling between shaft-bending and blade vibrations through less or more simplified models and concluded that coupling has substantial effect on certain natural frequencies of the system. In another study concerning a turbine-generator set of a power plant, Okabe et al. [8] considered the torsional vibrations of the finite element modelled shaft (A problem of special importance for that kind of system where electromagnetic torque disturbances excite torsional vibrations in the shaft.), represented the blades by equivalent spring–mass systems and reported that the coupled model has accurately predicted some of the natural frequencies of the actual system. Similarly, Huang and Ho [9] considered the eigenanalysis problem of coupled shaft-torsion and blade-bending vibrations in a rotor carrying a single bladed disk assembly via a mixed weighted residual—receptance method, modelled the blades as Euler–Bernouilli beams, and concluded that at some critical speeds the system would suffer loss of stability (a conclusion not supported by the present study, as will be apparent later on). Finally, in their recent work, Chatelet et al. [10] introduced two reduction techniques; to study the behaviour of a whole finite element modelled turbomachine and again concluded that coupling has substantial effects on certain natural frequencies of the system.

Although a geometrically accurate modelling and, therefore, an essentially numerical modelling approach of real bladed-rotor assemblies is indispensable for practising engineers in charge of production, it may be commented after Srinavasan [1] that it is also important to develop essentially analytical approaches, based on abstractions and idealizations, to form a necessary background for verifying and interpreting the results coming from essentially numerical ones and to provide a better insight into the problem, making it possible new and better numerical approaches to be developed. This constitutes the starting point of the present paper, which aims to a qualitative study of the coupling effects between shaft-torsional and blade-(in plane) bending vibrations in single and multi-stage rotor-blade systems. To this end, an idealized model consisting in a torsionally elastic shaft carrying a number of rigid discs, which in their turn, carry a number of identical (tuned) blades modelled as cantilevered Euler–Bernouilli beams is considered. The model is a multi-stage version of the one used in Ref. [9] and constitutes an extension of the somewhat abstract model consisting in a single blade (beam) attached to a rotating rigid disk considered by many authors among which are Southwell and Gaugh [11], Peters [12], Fox and Burdess [13], Wright et al. [14], and Naguleswaran [15]. To obtain the equations of motion of this multi-continuous-body system, a synthetical (parts are considered first), multi-frame (the motion of each part is referred to the computationally most favourable frame) and mixed (different modelling methods and consequently different types of coordinates are used for each part) approach is adopted. Specifically, finite element method is used to obtain a discrete model for the shaft and Galerkin's method is used to obtain a similar model for the blades. The resulting equations of motion are linear in shaft's torsional coordinates, nonlinear in blades' bending coordinates, and include both linear and nonlinear coupling between them. A consistent small vibrations assumption leads then to a fully linear model. It is shown that the related eigenanalysis problem splits into two independent sub-problems corresponding to two kinds of possible normal mode motions of the system. These are referred to as ''coupled shaft-torsion–blade-bending modes'' and ''rigid shaft modes'' by the authors. It is also shown that the eigenfrequencies pertaining to the coupled shaft-torsion–blade-bending modes are subject to eigenvalue loci veering phenomena, which makes the coupling to have drastic effects on the vibration characteristics of the system at certain combinations of the design parameters and operating conditions. It is also shown that the dimensions of the sub-problems do not depend on the blade number on each disk, making it possible a substantial dimension saving especially for systems with high number of blades.

2. The mathematical model

Consider Fig. 1a depicting a torsionally elastic shaft with mass density ρ_0, shear modulus G, polar area moment of inertia I_p and length ℓ_0 whose left end rotates at a constant rate Ω_0 and who carries a number p of bladed rigid disks. The ith disk has radius r_i and mass moment of inertia J_i and carries k_i identical (tuned) blades modelled as uniform Euler–Bernouilli beams of mass density ρ_i, flexural rigidity $(EI)_i$, cross-sectional area A_i, and length ℓ_i undergoing bending vibrations in the rotation plane.

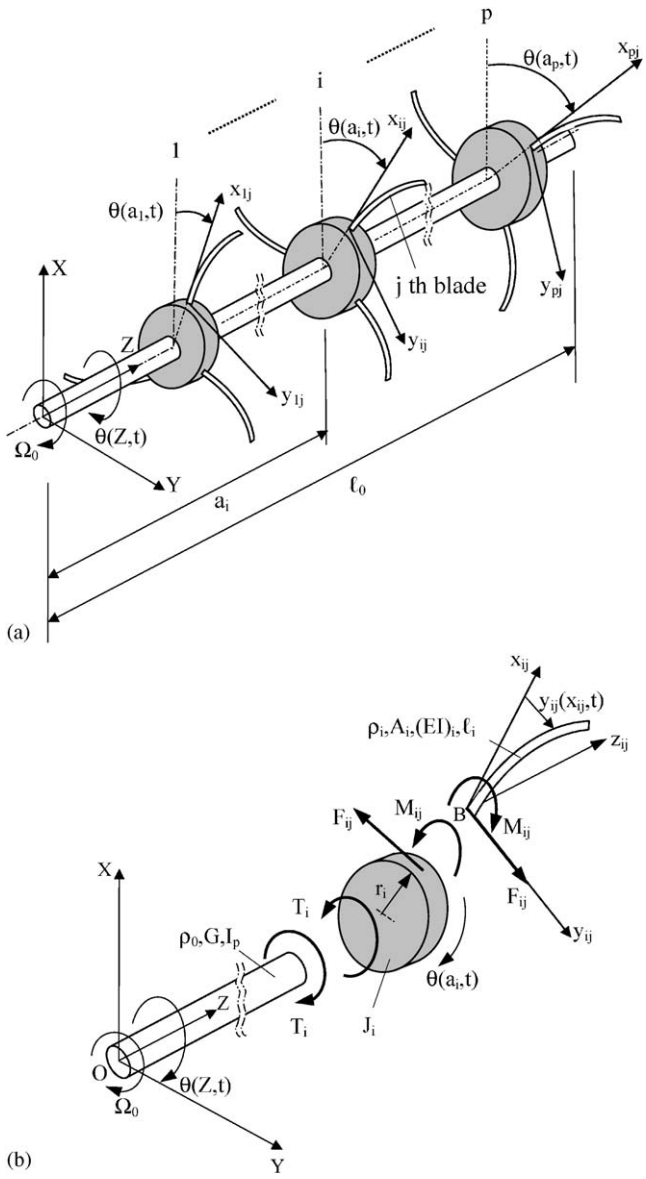

Fig. 1. The system: (a) general view; (b) elements.

To obtain the equations of motion of this system, which is a combined dynamic system consisting of three kinds of element, i.e. the shaft, the rigid disks and the blades (Fig. 1b) let a synthetical, multi-frame and mixed approach be adopted. Accordingly, consider first the three elements separately and select the most convenient frame of reference as well as the most convenient modelling method for each element.

Thus, consider first the torsionally elastic shaft acted upon by the reaction torque T_i of the ith disk, let its motion be referred to the frame $O;XYZ$ attached to the left end of the shaft (rotating at constant rate Ω_0), and let a discrete model of it be obtained via finite element method. Accordingly, divide the shaft into n elements with equal lengths, each possessing three nodes one of which is an internal node placed at the middle, adopt a quadratic interpolation scheme, and obtain

$$\rho_0 I_p \ell_0 \cdot \mathbf{M} \cdot \frac{\mathrm{d}^2\boldsymbol{\theta}}{\mathrm{d}t^2} + \frac{GI_p}{\ell_0} \cdot \mathbf{K} \cdot \boldsymbol{\theta} = \sum_{i=1}^{p} \mathbf{e}_{s_i} \cdot T_i, \tag{1}$$

where $\boldsymbol{\theta} = \{\theta_1, \theta_2, \ldots, \theta_{2n}\}^{\mathrm{T}}$is the $2n$-dimensional nodal torsional coordinates vector, $\mathbf{e}_j$ is the jth $2n$-dimensional unit vector such as $\mathbf{e}_3 = \{0, 0, 1, 0, \ldots, 0\}^{\mathrm{T}}$for example, s_i is the attachment station of the ith disk and $\rho_0 I_p \ell_0 \cdot \mathbf{M}$ and $GI_p/\ell_0 \cdot \mathbf{K}$ are $2n \times 2n$ consistent, global mass and stiffness matrices obtained by taking into account that the left end of the shaft is fixed to the frame and the right end is free. The structures of the matrices $\mathbf{M}$ and $\mathbf{K}$ are given in Appendix A.

Next consider the ith rigid disk acted upon by the reaction torque $-T_i$ of the shaft and the reaction forces $-F_{ij}$ and torques $-M_{ij}$; $j = 1, 2, \ldots, k_i$ of the k_i blades it carries, note that the disk shares the motion of the s_ith station of the shaft and obtain its equation of motion relative to the rotating frame $O;XYZ$ as

$$J_i \cdot \left(\mathbf{e}_{s_i}^T \cdot \frac{\mathrm{d}^2\boldsymbol{\theta}}{\mathrm{d}t^2}\right) = -T_i - \sum_{j=1}^{k_i}(r_i F_{ij} + M_{ij}). \tag{2}$$

Finally consider the jth blade (beam) of the ith disk and let the equation of motion of its in-plane, transverse vibrations relative to the moving frame $B;x_{ij}y_{ij}z_{ij}$ attached to the ith rigid disk be obtained. To this end, notice first that the vibrations of a stationary, uniform Euler–Bernouilli beam subjected to a distributed force whose axial and transversal components are given, respectively, as $f_x(x,t)$ and $f_y(x,t)$ is governed by the integro-partial differential equation

$$\mathrm{EI}\frac{\partial^4 y(x,t)}{\partial x^4} + \rho A \frac{\partial^2 y(x,t)}{\partial t^2} - \left[\int_x^{\ell} f_x(\xi,t)\,\mathrm{d}\xi\right]\frac{\partial^2 y(x,t)}{\partial x^2} + f_x(x,t)\frac{\partial y(x,t)}{\partial x} - f_y(x,t) = 0, \tag{3}$$

where EI is the flexural rigidity, A the cross-section area, ρ the mass density, ℓ the length of the beam, and ξ is a dummy variable standing for x. (See Appendix B for the derivation of this equation.) Then, substitute for $f_x(x,t)$ and $f_y(x,t)$ the corresponding components of the inertia force due to the motion of the frame $B;x_{ij}y_{ij}z_{ij}$, acting on a segment of unit length situated at point x_{ij} of the beam, vis.

$$\begin{aligned} f_x(x_{ij},t) &= \rho_i A_i\left[\Omega_i^2(r_i + x_{ij}) + \tfrac{\mathrm{d}\Omega_i}{\mathrm{d}t}y_{ij}(x_{ij},t) + 2\Omega_i\tfrac{\partial y_{ij}(x_{ij},t)}{\partial t}\right],\\ f_y(x_{ij},t) &= \rho_i A_i\left[\Omega_i^2 y_{ij}(x_{ij},t) - \tfrac{\mathrm{d}\Omega_i}{\mathrm{d}t}(r_i + x_{ij})\right], \end{aligned} \tag{4}$$

where Ω_i is the absolute angular velocity of the frame, i.e.

$$\Omega_i = \Omega_0 + \mathbf{e}_{s_i}^{\mathrm{T}} \cdot \frac{\mathrm{d}\boldsymbol{\theta}}{\mathrm{d}t}, \tag{5}$$

to obtain after some calculation

$$\begin{aligned} &(\mathrm{EI})_i\frac{\partial^4 y_{ij}}{\partial x_{ij}^4} + \rho_i A_i \frac{\partial^2 y_{ij}}{\partial t^2}\\ &\quad - \rho_i A_i \Omega_i^2\left\{\left[r_i(\ell_i - x_{ij}) + \frac{1}{2}\left(\ell_i^2 - x_{ij}^2\right)\right]\frac{\partial^2 y_{ij}}{\partial x_{ij}^2} - (r_i + x_{ij})\frac{\partial y_{ij}}{\partial x_{ij}} + y_{ij}\right\} + \rho_i A_i \frac{\mathrm{d}\Omega_i}{\mathrm{d}t}(r_i + x_{ij})\\ &\quad - \rho_i A_i\left\{\int_{x_{ij}}^{\ell_i}\left[\frac{\mathrm{d}\Omega_i}{\mathrm{d}t}y_{ij}(\xi,t) + 2\Omega_i\frac{\partial y_{ij}(\xi,t)}{\partial t}\right]\mathrm{d}\xi\right\}\frac{\partial^2 y_{ij}}{\partial x_{ij}^2} + \rho_i A_i\left[\frac{\mathrm{d}\Omega_i}{\mathrm{d}t}y_{ij} + 2\Omega_i\frac{\partial y_{ij}}{\partial t}\right]\cdot\frac{\partial y_{ij}}{\partial x_{ij}} = 0. \end{aligned} \tag{6}$$

Now, insert Eq. (5) into Eq. (6), assume that the amplitudes of the beam vibrations remain small so that the terms which are nonlinear in y_{ij} can be neglected, and obtain

$$\begin{aligned} &\rho_i A_i\frac{\partial^2 y_{ij}}{\partial t^2} + (\mathrm{EI})_i\frac{\partial^4 y_{ij}}{\partial x_{ij}^4} - \rho_i A_i\left(\Omega_0 + \mathbf{e}_{s_i}^{\mathrm{T}}\cdot\frac{\mathrm{d}\boldsymbol{\theta}}{\mathrm{d}t}\right)^2\left\{\left[r_i(\ell_i - x_{ij}) + \frac{1}{2}\left(\ell_i^2 - x_{ij}^2\right)\right]\frac{\partial^2 y_{ij}}{\partial x_{ij}^2} - (r_i + x_{ij})\frac{\partial y_{ij}}{\partial x_{ij}} + y_{ij}\right\}\\ &\quad + \rho_i A_i(r_i + x_{ij})\mathbf{e}_{s_i}^{\mathrm{T}}\cdot\frac{\mathrm{d}^2\boldsymbol{\theta}}{\mathrm{d}t^2} = 0. \end{aligned} \tag{7}$$

Eq. (7) shows that both linear and nonlinear coupling exists between the transverse vibrations of the blade and the torsional vibrations of the shaft–disk system. Although the effect of the nonlinear coupling, which may be

a source of instability for the vibrations of the blades (see Refs. [16,17]) deserves a separate study, in consistency with the above assumption about the vibration amplitudes of the beam, it will be assumed in this study that the term $\mathbf{e}_{s_i}^{\mathrm{T}} \cdot (\mathrm{d}\boldsymbol{\theta}/\mathrm{d}t)$ i.e. the vibration amplitudes of the rigid disks and their frequency are small enough so that the nonlinear coupling can be neglected. This yields in dimensionless form

$$\ddot{v}_{ij} + \eta_i^2 \cdot v_{ij}^{iv} - \beta^2 \left\{ \left[\alpha_i(1-u_{ij}) + \frac{1}{2}(1-u_{ij}^2) \right] v_{ij}'' - (\alpha_i + u_{ij}) v_{ij}' + v_{ij} \right\} + (\alpha_i + u_{ij}) \cdot \mathbf{e}_{s_i}^{\mathrm{T}} \cdot \ddot{\boldsymbol{\theta}} = 0, \tag{8}$$

where

$$u_{ij} = \frac{x_{ij}}{\ell_i}, \quad v_{ij} = \frac{y_{ij}}{\ell_i}, \quad \tau = \omega_i^* t, \quad \alpha_i = \frac{r_i}{\ell_i}, \quad \beta = \frac{\Omega_0}{\omega_i^*}, \quad \omega_i^* = \sqrt{\frac{(\mathrm{EI})_i}{\rho_i A_i \ell_i^4}}, \quad \eta_i = \frac{\omega_i^*}{\omega_i^*} \tag{9}$$

and overdots represent differentiation w.r.t. τ while primes representing differentiation w.r.t. u_{ij}. Note that the time is non-dimensionalized by using the frequency scale ω_i^* of the blades of the first disk and that the equation of motion of the blades of the ith disk is brought to that time scale by means of the frequency scales ratio η_i.

The selected reference frames are such that the accompanying boundary conditions are simply those of a fixed–free beam,

$$v_{ij}(0,\tau) = v_{ij}'(0,\tau) = v_{ij}''(1,\tau) = v_{ij}'''(1,\tau) = 0. \tag{10}$$

The boundary-value problem defined in Eqs. (8)–(10) may conveniently be approximated by a finite set of ordinary differential equations by means of Galerkin's method. To this end, introduce the m-term Galerkin series

$$v_{ij}(u_{ij},\tau) = \sum_{k=1}^{m} g_{ijk}(\tau) \cdot \varphi_k(u_{ij}), \tag{11}$$

use the orthonormal set of eigenfunctions

$$\varphi_k(u_{ij}) = \cosh\,\lambda_k u_{ij} - \cos\,\lambda_k u_{ij} - \kappa_k \cdot (\sinh\,\lambda_k u_{ij} - \sin\,\lambda_k u_{ij}), \quad \kappa_k = \frac{\cosh\,\lambda_k + \cos\,\lambda_k}{\sinh\,\lambda_k + \sin\,\lambda_k} \tag{12}$$

of a stationary cantilever as the set of comparison functions (the first five eigenvalues λ_k are given in Appendix C), follow the usual procedures of Galerkin's method to obtain in matrix–vector form

$$\ddot{\mathbf{g}}_{ij}(\tau) + \lfloor \eta_i^2 \cdot \boldsymbol{\Lambda}^4 - \beta^2 \cdot (\alpha_i \cdot \mathbf{A} + \mathbf{B} + \mathbf{I}) \rfloor \cdot \mathbf{g}_{ij}(\tau) + (\alpha_i \cdot \mathbf{c} + \mathbf{d}) \cdot \mathbf{e}_{s_i}^{\mathrm{T}} \cdot \ddot{\boldsymbol{\theta}}(\tau) = \mathbf{0}, \tag{13}$$

where $\boldsymbol{\Lambda}$ is a $m \times m$ diagonal matrix with elements $\Lambda_{rr} = \lambda_r$, $\mathbf{I}$ is the $m \times m$ unit matrix, $\mathbf{g}_{ij}(\tau)$ is the m-dimensional Galerkin coordinates vector of the related blade, $\mathbf{A}$ and $\mathbf{B}$ are $m \times m$ symmetrical matrices and $\mathbf{c}$ and $\mathbf{d}$ are m-dimensional vectors whose elements are defined as

$$\begin{gathered} A_{rs} = \int_0^1 \left[(1-u_{ij})\varphi_r'' - \varphi_r' \right] \cdot \varphi_s \cdot \mathrm{d}u_{ij}, \quad B_{rs} = \int_0^1 \left[\tfrac{1}{2}(1-u_{ij}^2)\varphi_r'' - u_{ij}\varphi_r' \right] \cdot \varphi_s \cdot \mathrm{d}u_{ij}, \\ c_r = \int_0^1 \varphi_r \cdot \mathrm{d}u_{ij}, \quad d_r = \int_0^1 u_{ij}\varphi_r \cdot \mathrm{d}u_{ij} \end{gathered} \tag{14}$$

and numerically given in Appendix C for $m = 5$. Let one also note that, on the basis of the foregoing analysis, the shearing forces F_{ij} and the bending moments M_{ij} exerted to the jth beam by the ith disk can be calculated as

$$F_{ij}(\tau) = \frac{(\mathrm{EI})_i \partial^3 v_{ij}(u_{ij},\tau)}{\ell_i^2 \quad \partial u_{ij}^3}\bigg|_{u_{ij}=0} = -2\frac{(\mathrm{EI})_i}{\ell_i^2}\mathbf{e}^{\mathrm{T}}\mathbf{g}_{ij}(\tau), \qquad M_{ij}(\tau) = -\frac{(\mathrm{EI})_i \partial^2 v_{ij}(u_{ij},\tau)}{\ell_i \quad \partial u_{ij}^2}\bigg|_{u_{ij}=0} = -2\frac{(\mathrm{EI})_i}{\ell_i^2}\mathbf{f}^{\mathrm{T}}\mathbf{g}_{ij}(\tau),$$

where $\mathbf{e}$ and $\mathbf{f}$ are m-dimensional vectors with elements

$$e_r = \kappa_r \lambda_r^3, \quad f_r = \lambda_r^2. \tag{16}$$

with κ_r as given in Eq. (12). Having thus obtained the equations of motion of the elements, it remains to synthesize them into that of the whole system. To this end, substitute first for F_{ij} and M_{ij} from Eq. (15) into Eq. (2) and then for T_i from Eq. (2) into Eq. (1) to obtain, after amening to the time scale τ and

non-dimensionalizing

$$\left(\mathbf{M}+\sum_{i=1}^{p}\gamma_i\cdot\mathbf{e}_{s_i}\mathbf{e}_{s_i}^{\mathrm{T}}\right)\cdot\ddot{\boldsymbol{\theta}}(\tau)+\mu^2\mathbf{K}\cdot\boldsymbol{\theta}(\tau)-\sum_{i=1}^{p}2\eta_i^2\delta_i\cdot\mathbf{e}_{s_i}\left(\alpha_i\cdot\mathbf{e}^{\mathrm{T}}+\mathbf{f}^{\mathrm{T}}\right)\cdot\left(\sum_{j=1}^{k_i}\mathbf{g}_{ij}(\tau)\right)=\mathbf{0},\tag{17}$$

where

$$\gamma_i=\frac{J_i}{\rho_0 I_p\ell_0},\quad \delta_i=\frac{\rho_i A_i\ell_i^3}{\rho_0 I_p\ell_0},\quad \mu=\frac{\omega_0^*}{\omega_1^*},\quad \omega_0^*=\sqrt{\frac{G}{\rho_0\ell_0^2}}.\tag{18}$$

Recasting Eqs. (17) and (13) into a single $2n+m\cdot\left(\sum_{i=1}^{p}k_i\right)$—dimensional hyper-matrix–vector equation one obtains finally

$$\begin{bmatrix}\mathbf{M}_{00}&\mathbf{0}&\mathbf{0}&\cdots&\mathbf{0}\\ \overline{\mathbf{M}}_{10}&\mathbf{I}&\mathbf{0}&\cdots&\mathbf{0}\\ \overline{\mathbf{M}}_{20}&\mathbf{0}&\mathbf{I}&\cdots&\mathbf{0}\\ \vdots&\vdots&\vdots&\ddots&\vdots\\ \overline{\mathbf{M}}_{p0}&\mathbf{0}&\mathbf{0}&\cdots&\mathbf{I}\end{bmatrix}\begin{Bmatrix}\ddot{\boldsymbol{\theta}}\\ \ddot{\mathbf{g}}_1\\ \ddot{\mathbf{g}}_2\\ \vdots\\ \ddot{\mathbf{g}}_p\end{Bmatrix}+\begin{bmatrix}\mathbf{K}_{00}&\delta_1\overline{\mathbf{K}}_{01}&\delta_2\overline{\mathbf{K}}_{02}&\cdots&\delta_p\overline{\mathbf{K}}_{0p}\\ \mathbf{0}&\overline{\mathbf{K}}_{11}&\mathbf{0}&\cdots&\mathbf{0}\\ \mathbf{0}&\mathbf{0}&\overline{\mathbf{K}}_{22}&\cdots&\mathbf{0}\\ \vdots&\vdots&\vdots&\ddots&\vdots\\ \mathbf{0}&\mathbf{0}&\mathbf{0}&\cdots&\overline{\mathbf{K}}_{pp}\end{bmatrix}\begin{Bmatrix}\boldsymbol{\theta}\\ \mathbf{g}_1\\ \mathbf{g}_2\\ \vdots\\ \mathbf{g}_p\end{Bmatrix}=\begin{Bmatrix}\mathbf{0}\\ \mathbf{0}\\ \mathbf{0}\\ \vdots\\ \mathbf{0}\end{Bmatrix},\tag{19}$$

where the vectors $\mathbf{g}_i$ are themselves hyper-vectors made up of the m-dimensional Galerkin coordinates' vectors of the k_i blades of the ith disk. Similarly the matrices $\overline{\mathbf{M}}_{i0}$ and $\overline{\mathbf{K}}_{0j}$ are hyper-matrices made up of k_i (or k_j) identical matrices and the matrices $\overline{\mathbf{K}}_{ii}$ are block-diagonal hyper-matrices with k_i identical diagonal blocks

$$\begin{gathered}\mathbf{g}_i=\left\{\mathbf{g}_{i1}^{\mathrm{T}}\quad\mathbf{g}_{i2}^{\mathrm{T}}\quad\cdots\quad\mathbf{g}_{ik_i}^{\mathrm{T}}\right\}^{\mathrm{T}},\quad\overline{\mathbf{M}}_{i0}=\left[\mathbf{M}_{i0}^{\mathrm{T}}\quad\mathbf{M}_{i0}^{\mathrm{T}}\quad\cdots\quad\mathbf{M}_{i0}^{\mathrm{T}}\right]^{\mathrm{T}},\\ \overline{\mathbf{K}}_{0j}=\lfloor\mathbf{K}_{0j}\quad\mathbf{K}_{0j}\quad\cdots\quad\mathbf{K}_{0j}\rfloor,\quad\overline{\mathbf{K}}_{ii}=\begin{bmatrix}\mathbf{K}_{ii}&\mathbf{0}&\cdots&\mathbf{0}\\ \mathbf{0}&\mathbf{K}_{ii}&\cdots&\mathbf{0}\\ \vdots&\vdots&\ddots&\vdots\\ \mathbf{0}&\mathbf{0}&\cdots&\mathbf{K}_{ii}\end{bmatrix}\end{gathered}\tag{20}$$

and where the $2n\times 2n$ matrices $\mathbf{M}_{00}$ and $\mathbf{K}_{00}$, $m\times m$ matrices $\mathbf{K}_{ii}$, $m\times 2n$ matrices $\mathbf{M}_{i0}$, and $2n\times m$ matrices $\mathbf{K}_{0j}$ are given as

$$\begin{gathered}\mathbf{M}_{00}=\mathbf{M}+\sum_{i=1}^{p}\gamma_i\cdot\mathbf{e}_{s_i}\mathbf{e}_{s_i}^{\mathrm{T}},\quad\mathbf{M}_{i0}=(\alpha_i\cdot\mathbf{c}+\mathbf{d})\cdot\mathbf{e}_{s_i}^{\mathrm{T}},\quad\mathbf{K}_{00}=\mu^2\mathbf{K},\\ \mathbf{K}_{0j}=-2\eta_j^2\mathbf{e}_{s_j}\left(\alpha_j\cdot\mathbf{e}^{\mathrm{T}}+\mathbf{f}^{\mathrm{T}}\right),\quad\mathbf{K}_{ii}=\eta_i^2\cdot\boldsymbol{\Lambda}^4-\beta^2\cdot(\alpha_i\cdot\mathbf{A}+\mathbf{B}+\mathbf{I}).\end{gathered}\tag{21}$$

As a clue for a ready interpretation of the foregoing mathematical description, note that the used matrix indices are given definite meanings. Thus, a zero index refers to the shaft while an index $i\neq 0$ referring to the ith blade-carrying disk. An index pair labels, therefore, a matrix that gathers the influences of the component pointed by the second index on the component pointed by the first one, as customary. Note also that all the hyper-matrices related to the blade-carrying disks have repetitive structures; a feature, which is an immediate result of the assumption about the similarity of the blades of a same disk.

Eq. (19) constitutes an approximate, discretisized and linearized equation of motion for the free vibrations of the multi-stage rotor-blade system shown in Fig. 1a.

3. Eigenanalysis

Introducing harmonic solutions in the form $\boldsymbol{\theta}(\tau)=\boldsymbol{\Theta}\cdot e^{i\sigma\tau}$, $\mathbf{g}_i(\tau)=\overline{\mathbf{G}}_i\cdot e^{i\sigma\tau}$; $\overline{\mathbf{G}}_i=\left\{\mathbf{G}_{i1}^{\mathrm{T}},\mathbf{G}_{i2}^{\mathrm{T}},\ldots,\mathbf{G}_{ik_i}^{\mathrm{T}}\right\}^{\mathrm{T}}$ into Eq. (19) and performing necessary matrix calculations by making use of the inversion and multiplication rules

of partitioned matrices [18,19], one is led to the eigenvalue analysis problem

$$\begin{bmatrix} \mathbf{A}_{00}-\sigma^2\mathbf{I} & \delta_1\cdot\overline{\mathbf{B}}_{01} & \delta_2\cdot\overline{\mathbf{B}}_{02} & \cdots & \delta_p\cdot\bar{\mathbf{B}}_{0p} \\ \overline{\mathbf{C}}_{10} & \overline{\mathbf{K}}_{11}+\delta_1\cdot\overline{\mathbf{D}}_{11}-\sigma^2\mathbf{I} & \delta_2\cdot\overline{\mathbf{D}}_{12} & \cdots & \delta_p\cdot\overline{\mathbf{D}}_{1p} \\ \overline{\mathbf{C}}_{20} & \delta_1\cdot\overline{\mathbf{D}}_{21} & \overline{\mathbf{K}}_{22}+\delta_2\cdot\overline{\mathbf{D}}_{22}-\sigma^2\mathbf{I} & \cdots & \delta_p\cdot\overline{\mathbf{D}}_{2p} \\ \vdots & \vdots & \vdots & \ddots & \vdots \\ \overline{\mathbf{C}}_{p0} & \delta_1\cdot\overline{\mathbf{D}}_{p1} & \delta_2\cdot\overline{\mathbf{D}}_{p2} & \cdots & \overline{\mathbf{K}}_{pp}+\delta_p\cdot\overline{\mathbf{D}}_{pp}-\sigma^2\mathbf{I} \end{bmatrix} \begin{Bmatrix} \mathbf{\Theta} \\ \overline{\mathbf{G}}_1 \\ \overline{\mathbf{G}}_2 \\ \vdots \\ \overline{\mathbf{G}}_p \end{Bmatrix} = \begin{Bmatrix} \mathbf{0} \\ \mathbf{0} \\ \mathbf{0} \\ \vdots \\ \mathbf{0} \end{Bmatrix}, \quad (22)$$

where the matrices with an over bar are hyper-matrices made up of k_i or $k_i \times k_j$ identical blocks with structures

$$\overline{\mathbf{B}}_{0j} = \lfloor \mathbf{B}_{0j} \quad \mathbf{B}_{0j} \quad \cdots \quad \mathbf{B}_{0j} \rfloor, \quad \overline{\mathbf{C}}_{i0} = \begin{bmatrix} \mathbf{C}_{i0} \\ \mathbf{C}_{i0} \\ \vdots \\ \mathbf{C}_{i0} \end{bmatrix}, \quad \overline{\mathbf{D}}_{ij} = \begin{bmatrix} \mathbf{D}_{ij} & \mathbf{D}_{ij} & \cdots & \mathbf{D}_{ij} \\ \mathbf{D}_{ij} & \mathbf{D}_{ij} & \cdots & \mathbf{D}_{ij} \\ \vdots & \vdots & \ddots & \vdots \\ \mathbf{D}_{ij} & \mathbf{D}_{ij} & \cdots & \mathbf{D}_{ij} \end{bmatrix}, \quad (23)$$

with

$$\mathbf{A}_{00} = \mathbf{M}_{00}^{-1}\mathbf{K}_{00}, \quad \mathbf{B}_{0j} = \mathbf{M}_{00}^{-1}\mathbf{K}_{0j}, \quad \mathbf{C}_{i0} = -\mathbf{M}_{i0}\mathbf{A}_{00}, \quad \mathbf{D}_{ij} = -\mathbf{M}_{i0}\mathbf{B}_{0j}. \quad (24)$$

Due to the repetitive structures of the involved hyper-matrices, this problem lends itself to further analytical development (see Appendix D) to yield the following results.

The frequency equation of the system may be written as

$$\det\left[\begin{bmatrix} \mathbf{A}_{00} & \Delta_1\mathbf{B}_{01} & \Delta_2\mathbf{B}_{02} & \cdots & \Delta_p\mathbf{B}_{0p} \\ \mathbf{C}_{10} & \Delta_1\mathbf{D}_{11}+\mathbf{K}_{11} & \Delta_2\mathbf{D}_{12} & \cdots & \Delta_p\mathbf{D}_{1p} \\ \mathbf{C}_{20} & \Delta_1\mathbf{D}_{21} & \Delta_2\mathbf{D}_{22}+\mathbf{K}_{22} & \cdots & \Delta_p\mathbf{D}_{2p} \\ \vdots & \vdots & \vdots & \ddots & \vdots \\ \mathbf{C}_{p0} & \Delta_1\mathbf{D}_{p1} & \Delta_2\mathbf{D}_{p2} & \cdots & \Delta_p\mathbf{D}_{pp}+\mathbf{K}_{pp} \end{bmatrix} - \sigma^2\mathbf{I}\right] \cdot \prod_{i=1}^{p}\left\{\det\left[\mathbf{K}_{ii}-\sigma^2\mathbf{I}\right]\right\}^{k_i-1} = 0, \quad (25)$$

where

$$\Delta_i = k_i\delta_i = k_i\frac{\rho_i A_i \ell_i^3}{\rho_0 I_p \ell_0} \quad (26)$$

is a dimensionless measure of the total rotary inertia of the ith disk's blades. Eq. (25) shows that the eigen analysis problem of the considered system splits into the following sub-problems.

(i) The coupled shaft-torsion–blade-bending modes sub-problem. The corresponding frequency equation is

$$\det\left[\begin{bmatrix} \mathbf{A}_{00} & \Delta_1\mathbf{B}_{01} & \Delta_2\mathbf{B}_{02} & \cdots & \Delta_p\mathbf{B}_{0p} \\ \mathbf{C}_{10} & \Delta_1\mathbf{D}_{11}+\mathbf{K}_{11} & \Delta_2\mathbf{D}_{12} & \cdots & \Delta_p\mathbf{D}_{1p} \\ \mathbf{C}_{20} & \Delta_1\mathbf{D}_{21} & \Delta_2\mathbf{D}_{22}+\mathbf{K}_{22} & \cdots & \Delta_p\mathbf{D}_{2p} \\ \vdots & \vdots & \vdots & \ddots & \vdots \\ \mathbf{C}_{p0} & \Delta_1\mathbf{D}_{p1} & \Delta_2\mathbf{D}_{p2} & \cdots & \Delta_p\mathbf{D}_{pp}+\mathbf{K}_{pp} \end{bmatrix} - \sigma^2\mathbf{I}\right] = 0. \quad (27)$$

The dimension of the sub-problem is $2n+pm$, implying that $2n+pm$ coupled modes exist irrespectively of the blade numbers k_i. Not only the eigenfrequencies, but also the eigenvectors of these modes can be calculated through the sub-problem of Eq. (27). To this end it suffices to note that the sth eigenvector

$$\mathbf{U}^{(s)} = \left\{\mathbf{\Theta}^{(s)^{\mathrm{T}}}, \mathbf{G}_{11}^{(s)^{\mathrm{T}}}, \mathbf{G}_{12}^{(s)^{\mathrm{T}}}, ..., \mathbf{G}_{1k_1}^{(s)^{\mathrm{T}}}, ..., \mathbf{G}_{p1}^{(s)^{\mathrm{T}}}, \mathbf{G}_{p2}^{(s)^{\mathrm{T}}}, ..., \mathbf{G}_{pk_p}^{(s)^{\mathrm{T}}}\right\}^{\mathrm{T}} \quad (28)$$

(corresponding to the sth eigenfrequency σ_s) of the main problem of Eq. (22) is related to the corresponding eigenvector

$$\mathbf{V}^{(s)} = \left\{ \mathbf{\Theta}^{(s)^{\mathrm{T}}}, \mathbf{G}_1^{(s)^{\mathrm{T}}}, \mathbf{G}_2^{(s)^{\mathrm{T}}}, ..., \mathbf{G}_p^{(s)^{\mathrm{T}}} \right\}^{\mathrm{T}} \tag{29}$$

of the sub-problem of Eq. (27) by

$$\mathbf{G}_{ij}^{(s)} = \mathbf{G}_i^{(s)}, \quad j = 2, 3, \ldots, k_i. \tag{30}$$

Literally, all the blades of a same disk behave in an exactly similar fashion in the coupled shaft-torsion–blade-bending modes, and this enables one to deduce the eigenvector of the original problem from that of the reduced order sub-problem.

(ii) The rigid shaft modes sub-problems. The corresponding frequency equations are

$$\det\lfloor \mathbf{K}_{ii} - \sigma^2 \mathbf{I} \rfloor = \det\lfloor \eta_i^2 \mathbf{\Lambda}^4 - \beta^2 \cdot (\alpha_i \cdot \mathbf{A} + \mathbf{B} + \mathbf{I}) - \sigma^2 \mathbf{I} \rfloor = 0, \quad i = 1, 2, \ldots, p. \tag{31}$$

Thus, to every blade-carrying disk there corresponds one such sub-problem, each of dimension m (i.e. the model degree-of-freedom of one blade) irrespectively of the blade number k_i. Noting that Eq. (31) is nothing but the frequency equation of the bending vibrations of a rotating blade attached to a rigid rotor (see Ref. [17], for example), one concludes that the shaft's torsional flexibility is of no consequences on (does not couple with) the related modes. As is clear from Eq. (25), each eigenvalue calculated from Eq. (31) is of multiplicity $(k_i - 1)$. This implies that these modes are peculiar to the systems where more than one blade exists on a disk. For these modes, an eigenvector $\mathbf{U}^{(s)}$ [see Eq. (28)] of the main problem of Eq. (22) can be calculated in terms of the corresponding eigenvector $\mathbf{W}_r^{(s)}$of the rth of the sub-problems of Eq. (31) by noting that

$$\mathbf{\Theta}^{(s)} = \mathbf{0}, \quad \mathbf{G}_{ij}^{(s)} = \begin{cases} \alpha_{rj}^{(s)} \cdot \mathbf{W}_r^{(s)}; \quad \sum_{j=1}^{k_r} \alpha_{rj}^{(s)} = 0 & \text{if} \quad i = r, \\ \mathbf{0} & \text{if} \quad i \neq r, \end{cases} \tag{32}$$

where $\alpha_{rj}^{(s)}$'s are (positive or negative) scaling factors. Thus, in a rigid shaft mode related to the rth disk, only the blades of that disk are vibrating (the blades mounted on other disks are at rest). The vibrating blades have all similar shapes but their vibrations are scaled so as to counter balance each other's effect on the disk. As a result, the shaft behaves as a rigid body in these modes. Note that Eq. (32) leaves an indefiniteness in the relative vibration amplitudes of the vibrating blades except when $k_i = 2$, where the two blades have the same amplitude but vibrate out-of-phase with respect to each other.

To summarize the results obtained in this section we note that the original $2n + m \cdot \left(\sum_{i=1}^{p} k_i\right)$ -dimensional eigenanalysis problem has been reduced into one sub-problem of dimension $2n + pm$ and p sub-problems of dimension m. Thus, the dependence of the dimension of the problem on the blade numbers k_i has been removed. Note that this corresponds to a considerable model reduction for systems with large number of blades. On the other hand, it is shown that the system has two kinds of normal mode motion. These are referred to as coupled shaft-torsion–blade-bending modes and rigid shaft modes by the authors. In the coupled shaft-torsion–blade-bending modes all the blades of a same disk behave in an exactly similar fashion. While in the rigid shaft modes, the entire shaft and the blades of all the disks except one are at rest. Each blade of the remaining disk vibrate as if it were attached to a rotating rigid shaft. The vibrating blades have all the same mode shapes but are scaled so that they are inter-balanced and their total effect on the disk vanishes.

4. Applications and results

This section is devoted to numerical application examples of the above presented analysis. The calculations are performed by means of a FORTRAN code developed for this purpose and in all the calculations $m = 10$ Galerkin terms are used to model a blade.

The alternative to the presented coupled analysis is to solve two separate uncoupled problems. These are the torsional vibrations problem of the shaft under the assumption that the blades are rigid, and that of the

bending vibrations of the rotating blades under the assumption that the shaft is rigid. The former problem may be written as

$$\left[\mathbf{M}+\sum_{i=1}^{p}\bar{\gamma}_i\mathbf{e}_{s_i}\mathbf{e}_{s_i}^{\mathrm{T}}\right]\cdot\ddot{\boldsymbol{\theta}}+\mu^2\mathbf{K}\cdot\boldsymbol{\theta}=\mathbf{0}, \tag{33}$$

where

$$\bar{\gamma}_i=\frac{\bar{J}_i}{\rho_0 I_p \ell_0}=\gamma_i+\Delta_i\left(\frac{1}{3}+\alpha_i^2+\alpha_i\right), \tag{34}$$

with

$$\bar{J}_i=J_i+k_i\rho_i A_i\ell_i\left[\frac{1}{12}\ell_i^2+\left(r_i+\frac{\ell_i}{2}\right)^2\right] \tag{35}$$

and the latter may be written as

$$\ddot{\mathbf{g}}_{ij}+\left[\eta_i^2\boldsymbol{\Lambda}^4-\beta^2\cdot(\alpha_i\cdot\mathbf{A}+\mathbf{B}+\mathbf{I})\right]\cdot\mathbf{g}_{ij}=\mathbf{0},\quad i=1,2,\ldots,p. \tag{36}$$

In order to give an idea on the effect of coupling, the results of these uncoupled problems will also be given along those of the coupled problem for each example.

4.1. Single-stage examples

We begin by investigating a single-stage rotor–blade system consisting in a shaft carrying a single bladed disk attached at its right end. Thus one has $p=1$ and the disk's attachment station number is $s=2n$. (In this section the indices i used to label quantities related to the ith disk will be dropped for convenience.) As the analysis does not depend on the number of blades, this number (k) needs not to be specified beforehand. In this section, where up to the 10th torsional frequency of the shaft will be of interest, $n=20$ finite elements are used to model the shaft, because numerical experiments have shown that this number is necessary if a satisfactory convergence is required in the 10th torsional frequency.

Validating the model: Before proceeding to the presentation of the application results of the above-presented model, it will be in order to check its validity. But as Eq. (31) is known to adequately model the vibrations of a rotating beam [17], only Eq. (27) needs to be checked. To this end, let one note that when the dimensionless parameter μ tends to zero the model will approach a torsionally elastic shaft-rigid blades model, and when μ tends to infinity it will approach a rigid shaft-flexible blades model. Eq. (27) can, therefore, be checked by comparing the results it yields at extreme values of μ, to the results obtained through corresponding limiting models.

Let one first consider the limiting case where μ tends to zero. In this case the model with k blades will approach that of a torsionally elastic shaft fixed at one end and carrying a rigid body of dimensionless mass moment of inertia $\bar{\gamma}$ [see Eq. (34)] at the other. It can be shown that the exact dimensionless natural frequencies of this model, which are defined as $\bar{\omega}_i=\omega_i/\omega_0^*$ [where ω_i's are the radial natural frequencies and ω_0^* is as given in Eq. (18)] are the roots of the transandantal equation

$$\cos\bar{\omega}-\bar{\gamma}\bar{\omega}\sin\bar{\omega}=0. \tag{37}$$

The first ten frequencies σ_i calculated from Eq. (27) with $\mu=0.0001$ are compared in Table 1 to those obtained from Eq. (37), after rescaling according to $\bar{\omega}_i=\sigma_i/\mu$. Comparisons are given for two different combinations of remaining system parameters: (a) $\alpha=0.4$, $\beta=0$, $\gamma=0.33$, $\Delta=0.75\rightarrow\bar{\gamma}=1$ and (b) $\alpha=0.4$, $\beta=0$, $\gamma=2.32$, $\Delta=3\rightarrow\bar{\gamma}=5$.

Next, the limiting case where μ tends to infinity is considered and the first three dimensionless natural frequencies $\sigma_i=\omega_i/\omega_1^*$ [where ω_1^* is as given in Eq. (9) and ω_i is the ith radial frequency] calculated from Eq. (27) with $\mu=10\,000$ are compared in Table 2 to those given by Naguleswaran ([15], Table 3, cl.-fr. boundary conditions) for the limiting rigid shaft-flexible blades model. Comparisons are presented for a dimensionless disk radius value of $\alpha=1$ and three different values of dimensionless rotation speed β. In the

Table 1
Comparison of the frequency calculations for $\mu = 0.0001$ to those of the elastic shaft-rigid blades model

		$\bar{\omega}_1$	$\bar{\omega}_2$	$\bar{\omega}_3$	$\bar{\omega}_4$	$\bar{\omega}_5$	$\bar{\omega}_6$	$\bar{\omega}_7$	$\bar{\omega}_8$	$\bar{\omega}_9$	$\bar{\omega}_{10}$
$\bar{\gamma} = 1$	Model	0.8620	3.4269	6.4381	9.5302	12.6471	15.7757	18.9127	22.0580	25.2132	28.3814
	Eq. (37)	0.8603	3.4256	6.4373	9.5293	12.6453	15.7713	18.9024	22.0365	25.1724	28.3096
$\bar{\gamma} = 5$	Model	0.4337	3.2042	6.3150	9.4464	12.5837	15.7248	18.8701	22.0213	25.1811	28.3527
	Eq. (37)	0.4328	3.2039	6.3148	9.4459	12.5823	15.7207	18.8602	22.0002	25.1407	28.2814

Table 2
Comparison of the frequency calculations for $\mu = 10\,000$ to those of the rigid shaft-elastic blades model (for $\alpha = 1$)

	$\beta = 0$			$\beta = 2$			$\beta = 10$		
	σ_1	σ_2	σ_3	σ_1	σ_2	σ_3	σ_1	σ_2	σ_3
Model	3.5160	22.0345	61.6972	4.4005	23.2803	63.0357	13.2591	43.2301	88.6025
Ref. [15]	3.5160	22.0345	61.6972	4.4005	23.2802	63.0358	13.2579	43.2266	88.5937

calculations, the remaining system parameters are set to $\gamma = 1$, $\Delta = 1$ and the results imported from Ref. [15], where they were given for out-of-rotation plane vibrations, are adapted to in-plane vibrations according to $\sigma_{\text{in}}^2 = \sigma_{\text{out}}^2 - \beta^2$. Note that for $\beta = 0$ the calculated frequencies also check with the squares of the frequencies λ_i given in Appendix C, as they should.

Inspection of Tables 1 and 2 shows that the performance of the presented model is satisfactory in the considered limiting cases. It may, therefore, be expected that it will remain so in the intermediate cases as well.

Parametric studies and results: The single-stage model depends only on the five dimensionless parameters α, β, γ, Δ and μ. In this section, parametric studies will be presented on the variation of the natural frequencies with these parameters.

Let first the effect of the dimensionless rotation speed β be examined and a system with $\alpha = 0.4$, $\gamma = 1$, $\Delta = 10$, $\mu = 10$ be considered for this purpose. The uncoupled frequencies are first calculated separately through Eqs. (33) and (36) and the results are plotted in Fig. 2a, where the horizontal lines are the torsional frequencies of the shaft (not affected by the rotation speed), and the curved lines are the bending frequencies of the blades (increasing with β due to centrifugal stiffening). Then, the coupled shaft-torsion–blade-bending frequencies are calculated from Eq. (27) and plotted in Fig. 2b. Note that, in view of the discussions of Section 3, this figure represents all the frequencies of a single-blade system. On the other hand, for a multi-blades system the rigid shaft frequencies of Eq. (31) have to be considered too. The result is Fig. 2c, which is nothing but a superposition of Fig. 2b and the blade frequency loci of Fig. 2a. To be precise, some calculated frequencies are also given numerically in Table 3. Comparing Figs. 2a and 2b one concludes that: i) The eigenfrequencies of the combined system is not much affected by the coupling at the parameter ranges away from the intersection points of the frequencies of the sub-systems taken separately. ii) Eigenvalue loci veering occur and, as a result, coupling has considerable effect on the eigenfrequencies (especially the lower ones) at the vicinity of these points. In order to see what physically happens in the loci veering regions, the coupled shaft-torsion–blade-bending mode shapes corresponding to different points of the loci A and B of Fig. 2c are calculated and presented in Fig. 3, where the modal displacement patterns of the shaft and blades are shown separately for ease of interpretation. Only one blade is considered on the figures because the blade shape is known to be independent of the blade number. Inspection of this figure shows that eigenvalue loci veering are accompanied with a gradual transition from one uncoupled mode to another. This, along with its own importance, can be viewed as a verification of the physical reality of the eigenvalue veering phenomenon, as discussed by Jei and Lee [20] in the context of the eigenvalue problem of continuous rotor-bearing systems.

It is also of interest to consider the rigid shaft modes. To this end, Fig. 4 is given where $(k-1)$ possible shapes corresponding to the first three modes of $k = 2$ and three bladed systems are presented for a

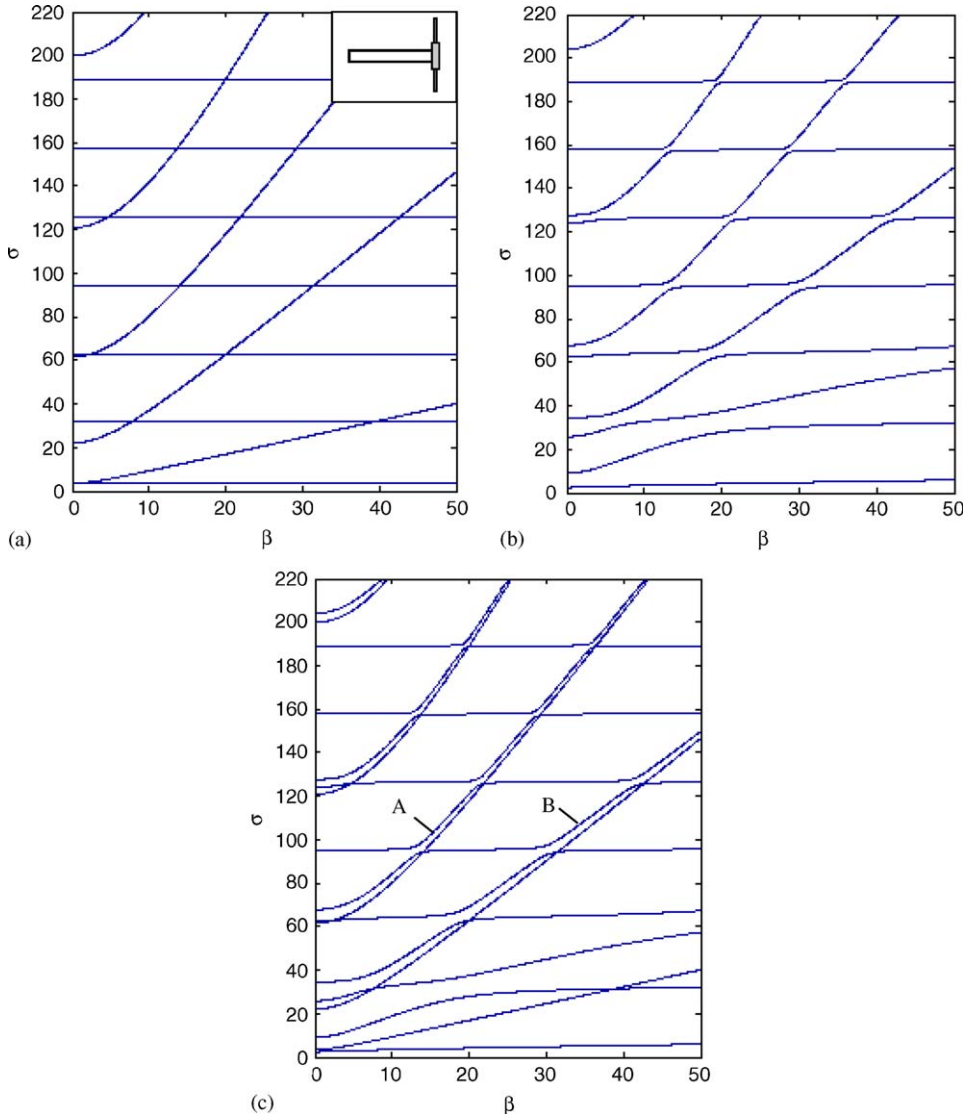

Fig. 2. Variation of the eigenfrequencies with the rotation speed, $\alpha = 0{\cdot}4$, $\gamma = 1$, $\Delta = 10$, $\mu = 10$: (a) uncoupled; (b) coupled; (c) all frequencies. In (a) horizontal lines, shaft-torsional; rising lines, blade-bending frequencies.

Table 3
Frequencies for a k-blades system

	σ_1	σ_2	σ_3	σ_4	σ_5	σ_6	σ_7	σ_8	σ_9	σ_{10}
$\beta = 0$	2.4147	3.5160*	9.0813	22.0345*	25.7803	34.4928	61.6972*	62.5385	67.7701	95.1458
$\beta = 5$	2.9264	5.6545*	12.6040	26.6164*	29.1079	35.7292	63.4377	66.8854*	71.8722	95.2172
$\beta = 10$	3.3873	9.2643*	18.8391	32.7712	37.0050*	42.7690	64.1111	80.2182*	84.1402	95.4932
$\beta = 15$	3.7511	13.0496*	24.3159	34.7057	49.5139*	54.1024	64.7881	94.7241	98.0155*	102.2744
$\beta = 20$	4.0905	16.8752*	27.8875	37.4354	62.8077*	62.8263	69.1592	95.2533	117.9818*	121.0768

$\alpha = 0.4$, $\gamma = 1$, $\Delta = 10$, $\mu = 10$, an asterisk shows a $(k-1)$-fold eigenvalue.

dimensionless rotation speed value of $\beta = 20$. The shaft's shape is not shown on these figures because the shaft is known to behave as a rigid body in these modes. Note that the given shapes are uniquely determined (up to a scaling factor) for $k = 2$ but that they only constitute possible examples for $k = 3$.

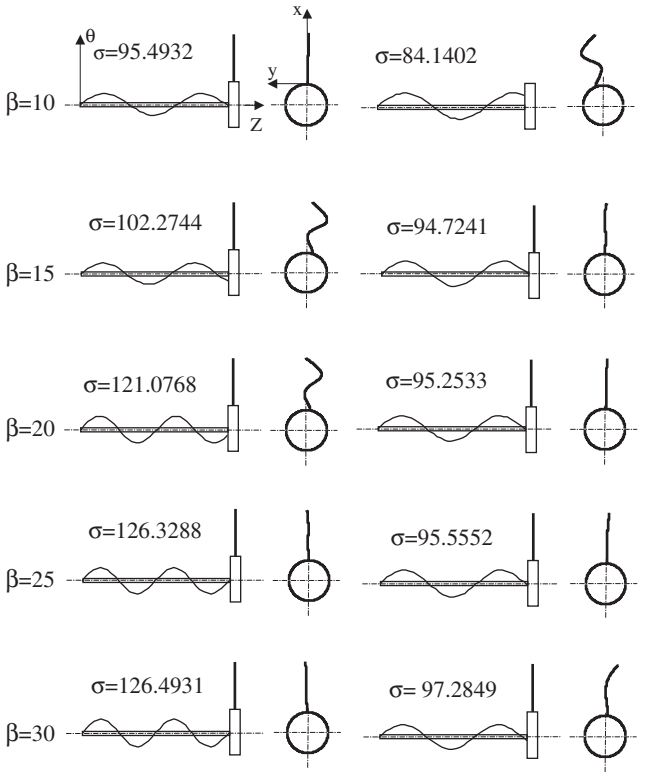

Fig. 3. Coupled shaft-torsion–blade-bending modes: transition from one uncoupled mode to another during eigenvalue loci veering. Left column, points on locus A; right column, points on locus B of Fig. 2c.

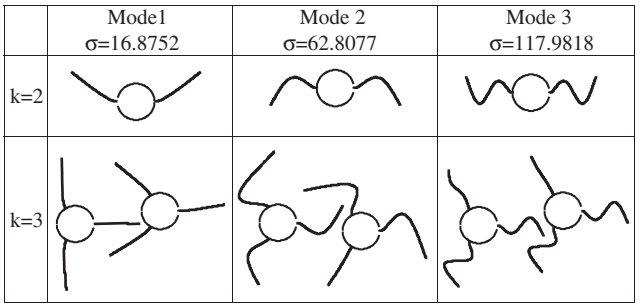

Fig. 4. Rigid shaft modes for $\beta = 20$.

Comparing the results obtained here to those obtained in Ref. [9], one notes that there are some similarities with respect to the obtained mode shapes, but the Figs. 2b and c depicting the variation of the eigenfrequencies with the rotation speed are in qualitative discrepancy with their counterparts in Ref. [9]. Although the authors could not perform an analysis on the very example of Ref. [9] due to missing data, they were unable to verify, on the basis of their own theoretical and numerical work, the statement of Ref. [9] about the existence of critical speeds where instabilities of flatter or of divergence type occur.

Second, let the effect of varying the dimensionless disk radius α be examined and let a system with $\beta = 10$, $\gamma = 1$, $\Delta = 1$, $\mu = 10$ be considered for this purpose. The uncoupled eigenfrequencies are plotted versus α in Fig. 5a, those obtained from Eq. (27) are plotted in Fig. 5b, and the combined results of Eqs. (27) and (31) are plotted in Fig. 5c. Thus, Fig. 5b represents the frequency variations of a single-blade system, while Fig. 5c represents those of a multi-blades one. Along with the parameter ranges where $\alpha > 0$, the ranges where $\alpha < 0$

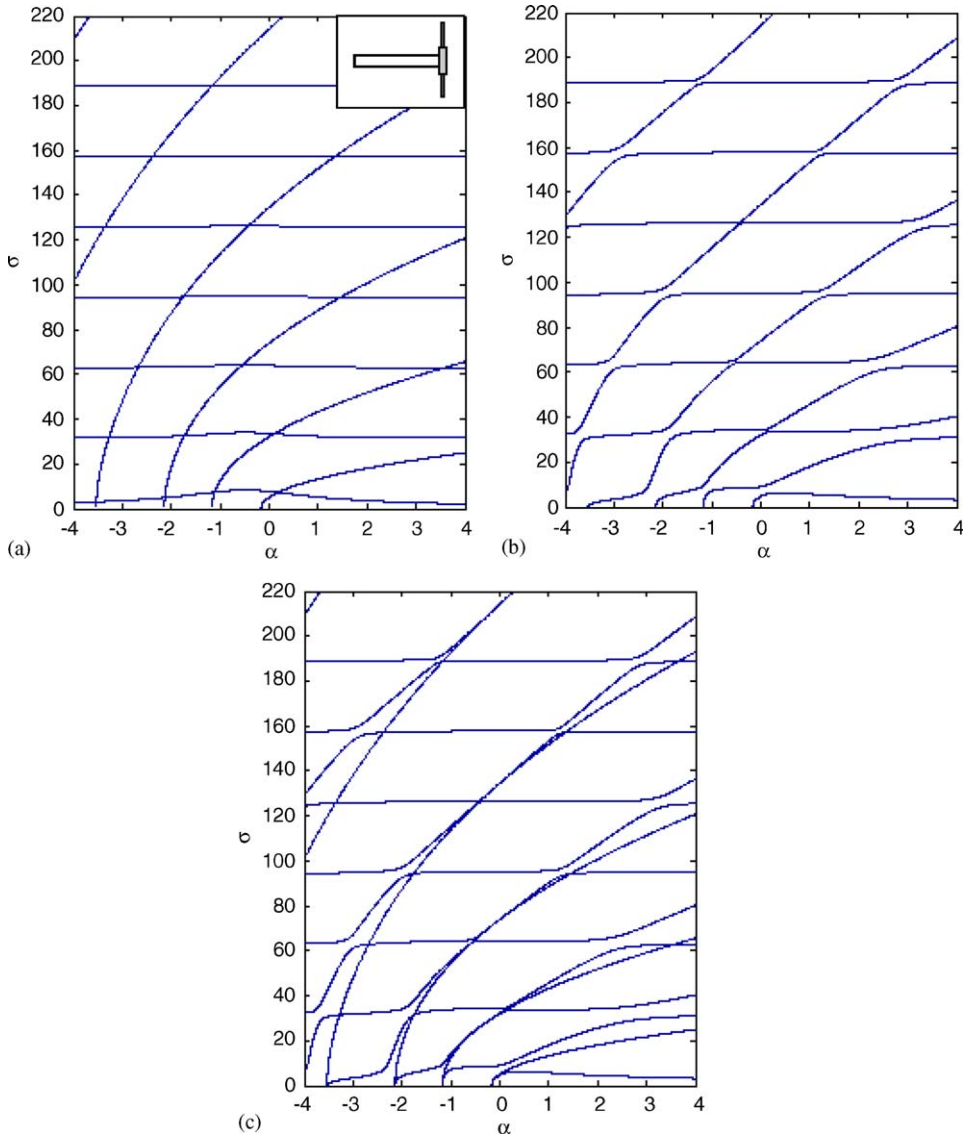

Fig. 5. Variation of the eigenfrequencies with the disk radius, $\beta = 10$, $\gamma = 1$, $\Delta = 1$, $\mu = 10$: (a) uncoupled; (b) coupled; (c) all frequencies.

(which correspond to rotor systems where the blades are oriented towards the centre of rotation) are also considered in these figures. The conclusions deduced from an inspection of these figures may be summarized as follows: (i) The frequencies corresponding to blade-bending modes increase with α due to the centrifugal stiffening effect (Fig. 5a), and eigenvalue loci veering occurs at the vicinity of the points where they would equal a frequency corresponding to a shaft-torsion mode (Figs. 5b, c). (ii) The frequencies corresponding to blade bending modes vanish at a certain value of α in the range where $\alpha < 0$. This is because an inward-oriented blade is under the compressive (softening) effect of the centrifugal forces and may suffer loss of static stability (buckling). This problem is introduced by Mostaghel and Tadjbakhsh [21] and subsequently treated by many authors; e.g. Peters and Hodges [22]. A vanishing frequency means buckling in the corresponding mode. It is interesting to note that the loci of uncoupled and coupled blade bending frequencies emanate from the same α values. Thus, coupling does not alter the buckling conditions and, therefore, need not to be considered in a buckling analysis.

Next, consider the effect of varying the dimensionless disk moment of inertia γ and consider a multi-blades system (blade number k) with $\alpha = 0{\cdot}4$, $\beta = 10$, $\Delta = 10$, $\mu = 10$ for this purpose. The result is presented in Fig. 6. The horizontal lines are the loci of the $(k-1)$-fold blade-bending frequencies corresponding to rigid shaft modes [Eq. (31)], which are not affected by the changes in γ. The remaining lines are the loci of the frequencies corresponding to coupled shaft-torsion–blade-bending modes [Eq. (27)]. Those approaching the horizontal ones with increasing γ are the loci of the coupled blade-bending frequencies. The reason for the two loci to approach is the weakening of the coupling with increasing disk inertia, which prevents the disk oscillations. Another result of this is the tendency of the shaft to a one with fixed–fixed boundary conditions. As a matter of fact, the loci of the coupled shaft-torsion frequencies, are seen to tend to the (rescaled) fixed–fixed rod frequencies $\sigma_i = \mu j\pi$; $j = 1,2,\ldots$, with increasing γ, except the lowest one which approaches zero.

Now, let the effect of varying the dimensionless measure $\Delta = k\delta$ of the total moment of inertia of the blades be examined. A multi-blades example with $\alpha = 0{\cdot}4$, $\beta = 10$, $\gamma = 1$, $\mu = 5$ is considered for this purpose and the

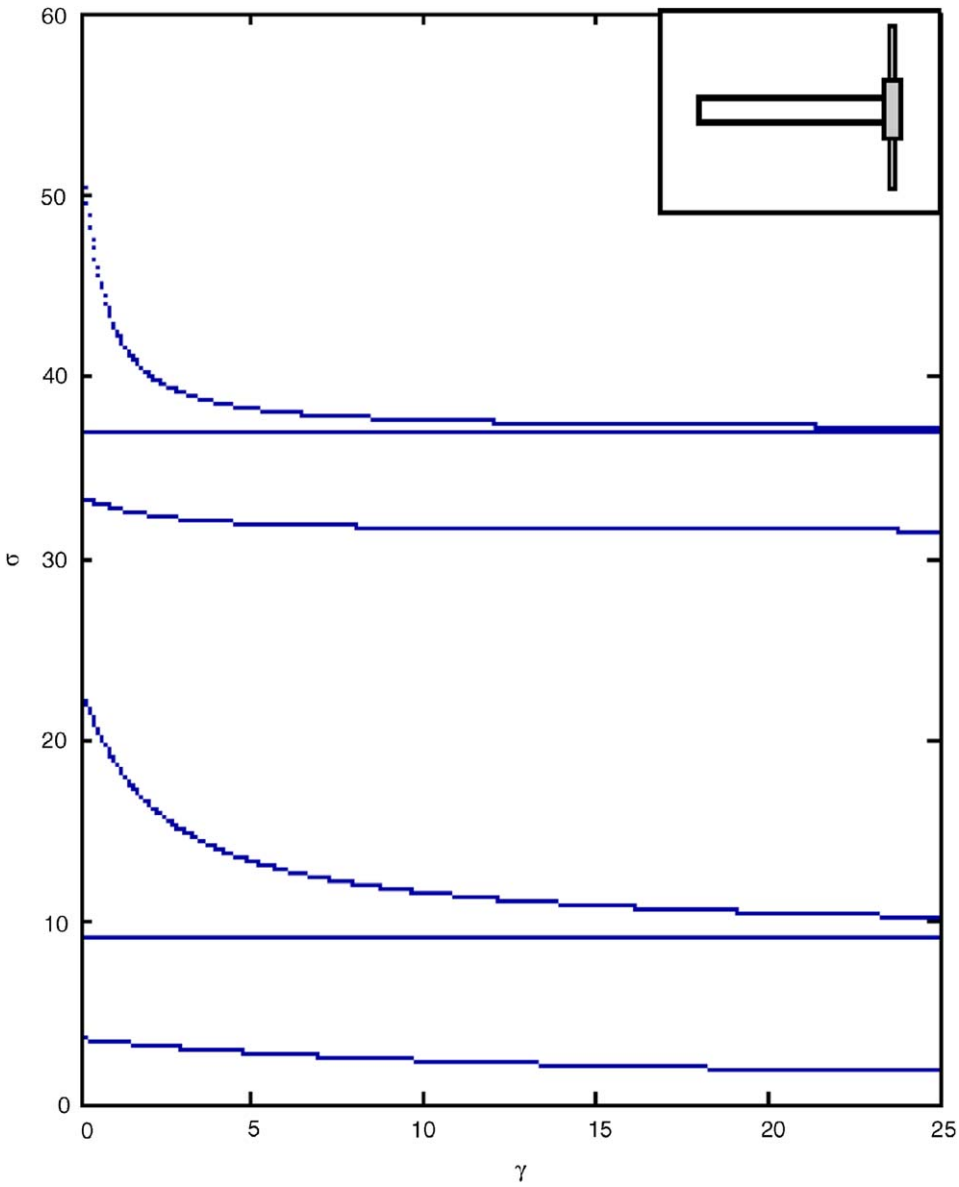

Fig. 6. Variation of the eigenfrequencies with the disk inertia ($\alpha = 0{\cdot}4$, $\beta = 10$, $\Delta = 10$, $\mu = 10$).

results are presented on Fig. 7. The horizontal lines on the figure represent the $(k-1)$-fold loci of the rigid shaft modes' blade-bending frequencies [Eq. (31)], which are not affected by the changes in Δ. The lines emanating from the same points as the horizontal ones at $\Delta = 0$ (i.e. when there is no coupling) but quickly departing from them when $\Delta \neq 0$ (i.e. when coupling occurs) are the loci of the coupled blade-bending frequencies. The remaining lines are the loci of the coupled shaft-torsional frequencies. As expected, (except the lowest one which approaches zero) they tend to the rescaled fixed–fixed rod frequencies $\sigma_i = \mu j\pi$; $j = 1,2,\ldots$, with increasing Δ. However, eigenvalue loci veering occur and coupled frequency l oci interchange their direction.

Finally, consider the effect of varying the ratio μ of the natural frequency scales of the shaft and the blades, and consider a multi-blades example with $\alpha = 0{\cdot}4$, $\beta = 10$, $\gamma = 1$, $\Delta = 2$ for this purpose. The results are presented in Fig. 8. The horizontal lines on the figure represent the $(k-1)$-fold loci of the rigid shaft modes' blade-bending frequencies (not affected by the changes in μ). The coupled shaft-torsion frequencies increase

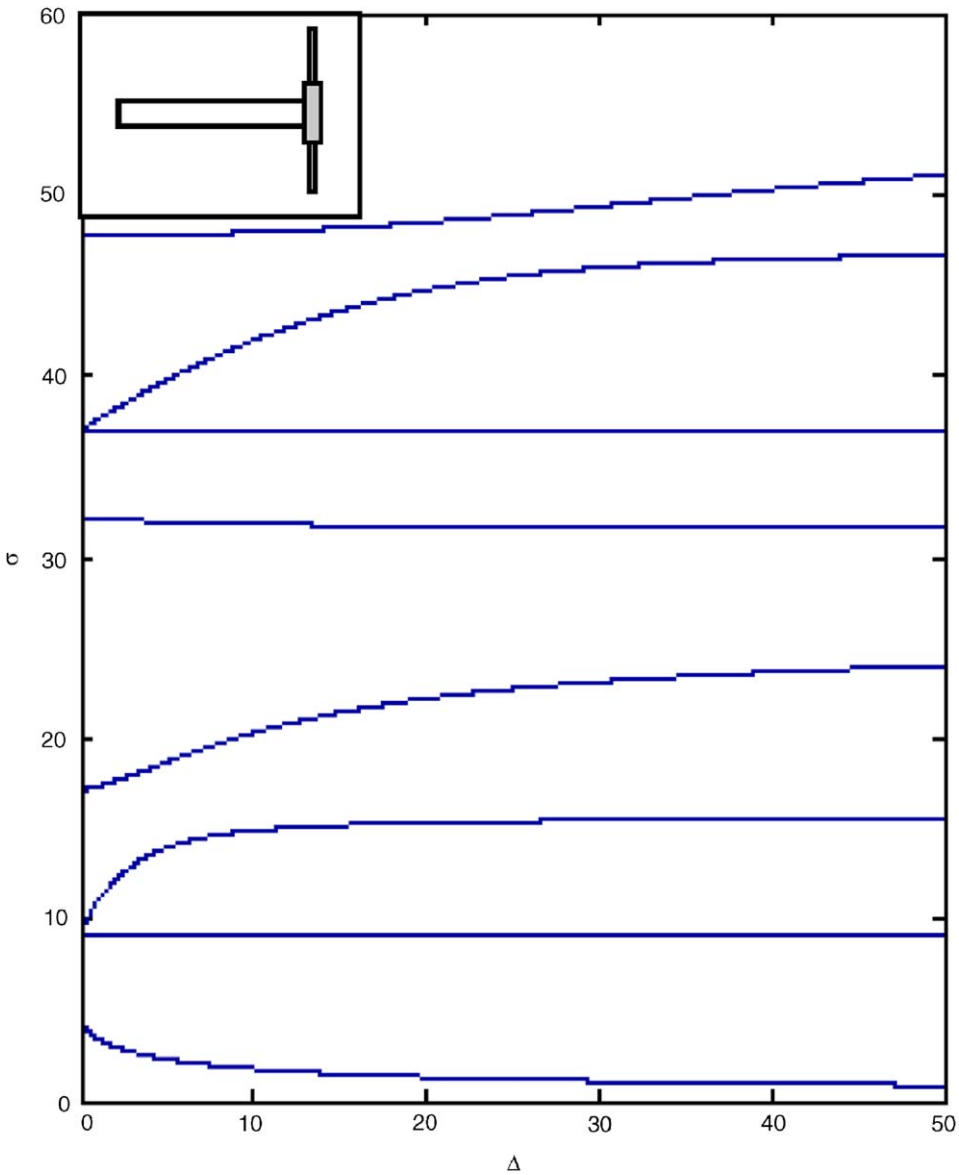

Fig. 7. Variation of the eigenfrequencies with the blades' total inertia ($\alpha = 0.4$, $\beta = 10$, $\gamma = 1$, $\mu = 5$).

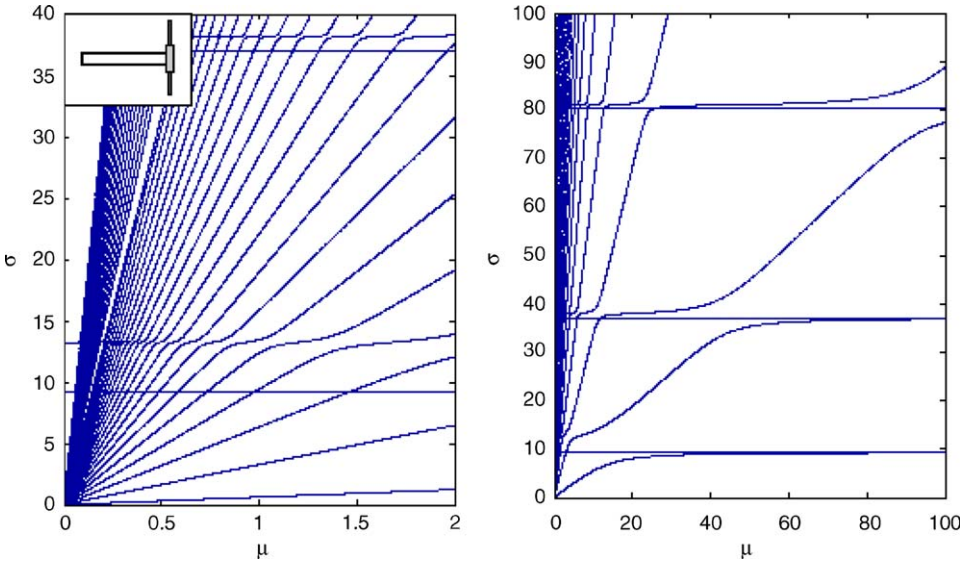

Fig. 8. Variation of the eigenfrequencies with the ratio of the natural frequency scales of the shaft and blades ($\alpha = 0.4$, $\beta = 10$, $\gamma = 1$, $\Delta = 2$).

linearly with μ, as they should. Their loci are seen to be involved in curve veering with the loci of the coupled blade-bending frequencies. Their general tendency is such that the system undergoes a transition from a flexible shaft-rigid blades system to a rigid shaft-flexible blade one with increasing μ.

4.2. Multi-stage examples

In this section, the presented analysis method will be applied to several multi-stage rotor-blade systems. After a number of numerical experiments, it is decided to use 10 finite elements for each shaft portion delimited by the disks to keep convergence guaranteed despite several discontinuities (disks) placed throughout. This amounts to $n = 10(p+1)$ finite elements for a shaft carrying p disks. The number k_i of the blades of the ith disk are again not specified beforehand.

Let first a hypothetical rotor-blade system with identical and equally spaced stages be considered so that the ith disk is placed at a distance $a_i = (\ell_0/p+1)\cdot i$ from the left end of the shaft, and the system data are given as $\mu = 5$, $\alpha_i = 1$, $\gamma_i = 0.2$, $\Delta_i = 0.4$, $\eta_i = 1$; $i = 1, 2, \ldots, p$. Let the variation of the eigenfrequencies with the dimensionless rotation speed β be obtained for systems with different number of stages. The results are presented in Figs. 9a–d corresponding to stage numbers $p = 2$, 3, 6 and 20, respectively. Figs. 9a1–d1 depict the uncoupled analysis results based on Eqs. (33) and (36) while Figs. 9a2–d2 depicting those of the coupled analysis based on Eqs. (27) and (31).

In Figs. 9a1–d1, the horizontal lines are the loci of the eigenfrequencies of the shaft's torsional vibrations, which are not affected by the rotation speed. Due to the lumped inertias of the attached disks and blades, the disk attachment points of the shaft have a tendency to stay at rest especially at higher frequencies. As a result, at higher modes, the shaft tends to behave as if it consisted of p fixed–fixed and one fixed–free rods, each of length $\ell_0/(p+1)$ with frequencies $\sigma_r = r(p+1)\mu\pi$ and $\sigma_r = (r-0.5)(p+1)\mu\pi$; $r = 1,2,\ldots$, respectively, where the scaling factor μ of Eq. (18) is taken into consideration. Accordingly, the shaft's torsional frequencies (except the p lower ones) are seen to consist of groups of p frequencies approaching $\sigma_r = r(p+1)\mu\pi$ and single values approaching $\sigma_r = (r-0.5)(p+1)\mu\pi$. On the other hand, the rising lines are the loci of the eigenfrequencies of the blades' in-plane bending vibrations (increasing with the rotation speed due to the stiffening effect of the centrifugal forces). It can be seen that the emanation points of these loci correspond to the dimensionless frequencies λ_i^2; $i = 1,2,\ldots$ of a stationary cantilever (see Appendix C), as they should.

Let Figs. 9a2–d2 depicting the coupled analysis results be considered now. Some conclusions, which can be drawn from an examination of these figures may be summarized as follows: (i) The loci of the uncoupled blade in-plane bending frequencies also subsist in the presence of coupling. In view of Eqs. (25) and (31), these frequencies are $p(k-1)$-fold for this example with p identical stages each carrying $k(\neq 1)$ blades. (ii) One blade-bending frequency for each stage couples with the shaft-torsional frequencies. Their loci form bundles of p lines lying about the loci of the corresponding uncoupled blade-bending frequency locus. (iii) The coupled blade-bending frequency loci involve in eigenvalue loci veering phenomena with the loci of the shaft torsional frequencies. As a result, the coupled frequency analysis results considerably depart from those of the uncoupled analysis.

For a second group of examples let a rotor-blade system with equally spaced, identical blade-carrying disks but different bladings at each stage be considered. The system data are generated from $\mu = 5$, $\alpha_1 = 1$, $\gamma_1 = 0.2$,

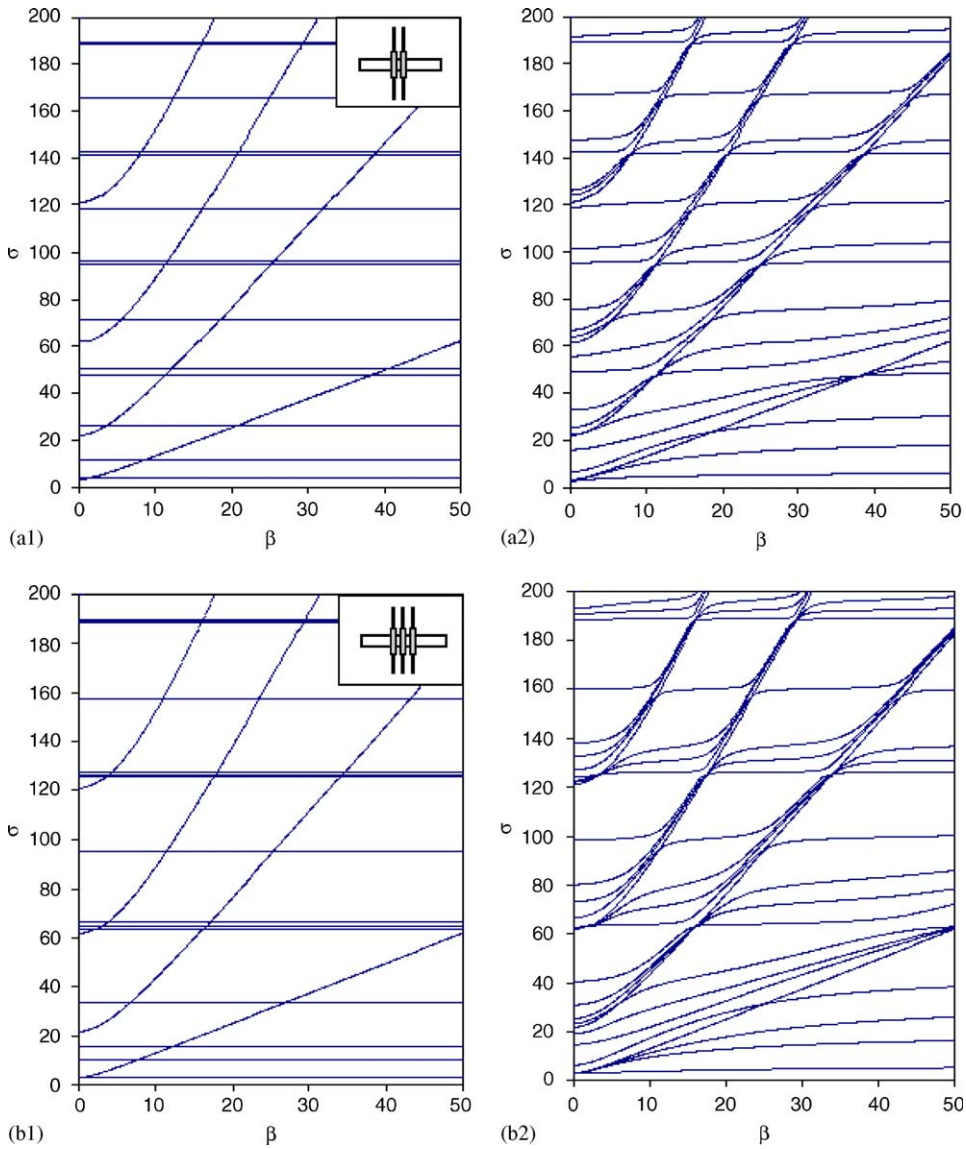

Fig. 9. Variation of the eigenfrequencies with the rotation speed. System with identical stages: (a) two; (b) three; (c) six; (d) twenty-stage system. Left-hand side, uncoupled; right-hand side, coupled analysis results.

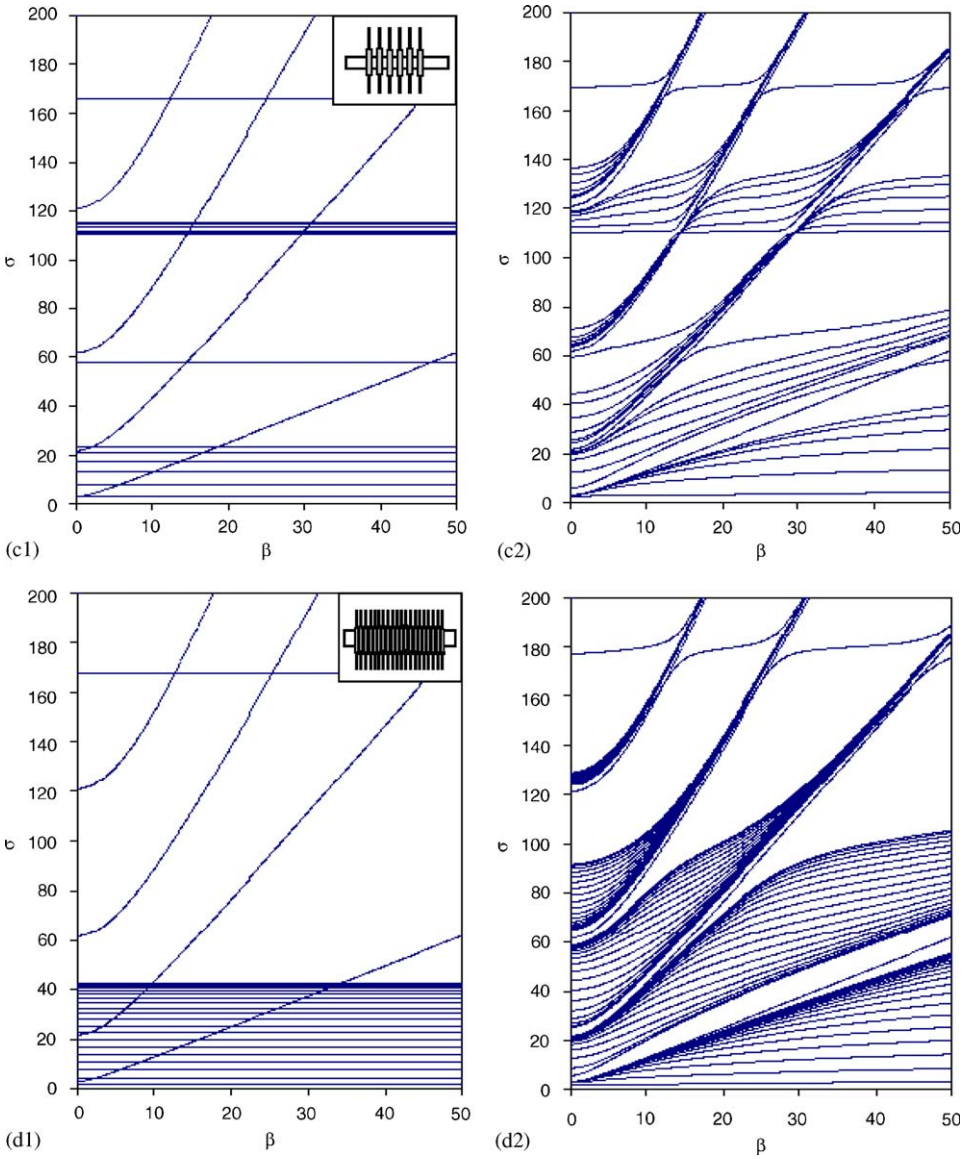

Fig. 9. (*Continued*)

$\Delta_1 = 0.4$, $\alpha_i = \alpha_1/\psi_i$, $\gamma_i = \gamma_1$, $\Delta_i = \Delta_1\psi_i^3$, $\eta_i = \eta_1/\psi_i^2$; $i = 2,3,\ldots,p$ with $\psi_i = 1 - 0.04(i-1)$ and the variation of the eigenfrequencies with the dimensionless rotation speed β is studied for systems with different number of stages. The results are presented in Figs. 10a–d corresponding again to stage numbers $p = 2$, 3, 6 and 20, respectively, and where, again, the uncoupled analysis results are also presented. An inspection of Figs. 10a1–d1 shows that the uncoupled blade-bending frequencies form groups of p frequencies, this being an obvious result of the fact that, in this example, different bladings with different frequency scales exist on each stage. Inspecting now Figs. 10a2–d2 depicting the coupled frequency analysis results one concludes that; (i) As a result of the spreading of the blade-bending frequencies related to different stages, the figures are now much more involved. (ii) As in the above example, the loci of the uncoupled blade in-plane bending frequencies subsist in the presence of coupling. But a locus corresponding to the ith stage is now (k_i-1)-fold. (iii) Again, one blade-bending frequency locus for each stage involves in loci veering phenomena with

shaft-torsional frequency loci and this makes the coupled analysis results to differ considerably from the uncoupled analysis ones. The discrepancies can also be seen in Table 4 where a first few coupled and uncoupled frequencies of the three-stage rotor-blade system of Fig. 10b are numerically given for three different values of the dimensionless rotation speed.

Finally, to give an idea on the coupled shaft-torsion–blade-bending mode shapes, three mode shape examples corresponding to the points A, B and C of the same veering eigenvalue locus of Fig. 10b2 are given in Fig. 11. This figure shows that a metamorphosis of the mode shape accompany the eigenvalue loci veering phenomena. As a matter of fact, the mode shape of Fig. 11a reflects a coupling between the 8th shaft-torsion mode and the 3rd blade-bending mode, that of Fig. 11b a coupling between the 11th shaft-torsion mode and the 3rd blade-bending mode, and that of Fig. 11c a coupling between the 11th shaft-torsion mode and the 2nd blade-bending mode, as should be expected in view of the locations of the points A, B and C in Fig. 10b2.

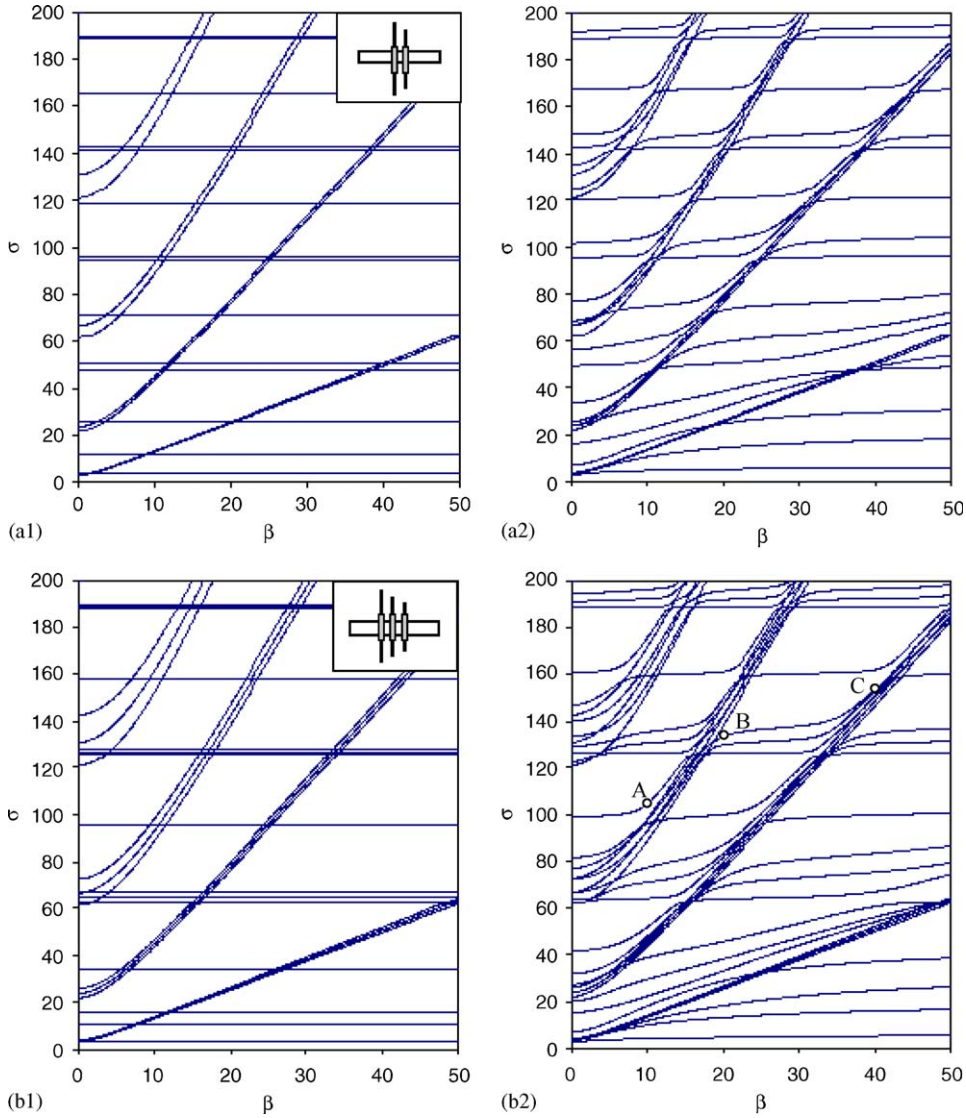

Fig. 10. Variation of the eigenfrequencies with the rotation speed. System with different stages: (a) two; (b) three; (c) six; (d) twenty-stage system. Left-hand side, uncoupled; right-hand side, coupled analysis results.

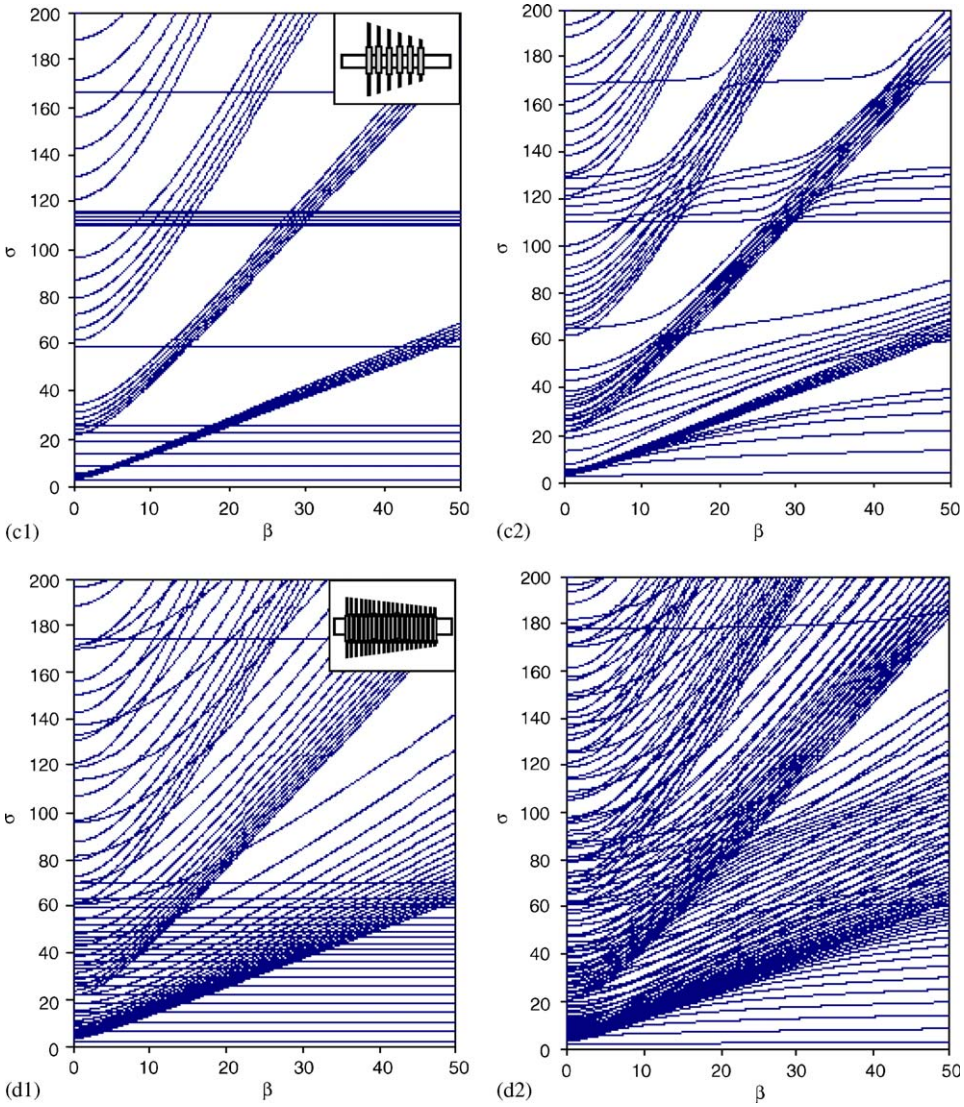

Fig. 10. (*Continued*)

Table 4
Comparison of the uncoupled and coupled frequency calculations for the three-stage system of Fig. 10b

		σ_1	σ_2	σ_3	σ_4	σ_5	σ_6	σ_7	σ_8	σ_9	σ_{10}
$\beta = 5$	Unc.	3.8217	7.4115	7.6742	7.9669	10.8356	16.2886	28.9241	30.5275	32.3645	34.2830
	Coupled	3.8066	6.7568	7.2713	7.4115^{1}	7.6742^{2}	7.9669^{3}	11.1726	17.5527	23.9908	28.9241^{1}
$\beta = 10$	Unc.	3.8217	10.8356	13.2591	13.6068	13.9819	16.2886	34.2830	43.2302	44.6464	46.2595
	Coupled	4.2432	10.0059	11.7896	13.2591^{1}	13.6068^{2}	13.9819^{3}	17.9819	22.1347	29.3416	38.5508
$\beta = 15$	Unc.	3.8217	10.8356	16.2886	19.2625	19.7228	20.2141	34.2830	59.5924	61.0254	62.6322
	Coupled	4.5405	11.9346	15.4188	19.2625^{1}	19.7228^{2}	20.2141^{3}	24.0817	27.4503	33.7671	42.0696

An upper index i shows a (k_i-1)-fold eigenvalue.

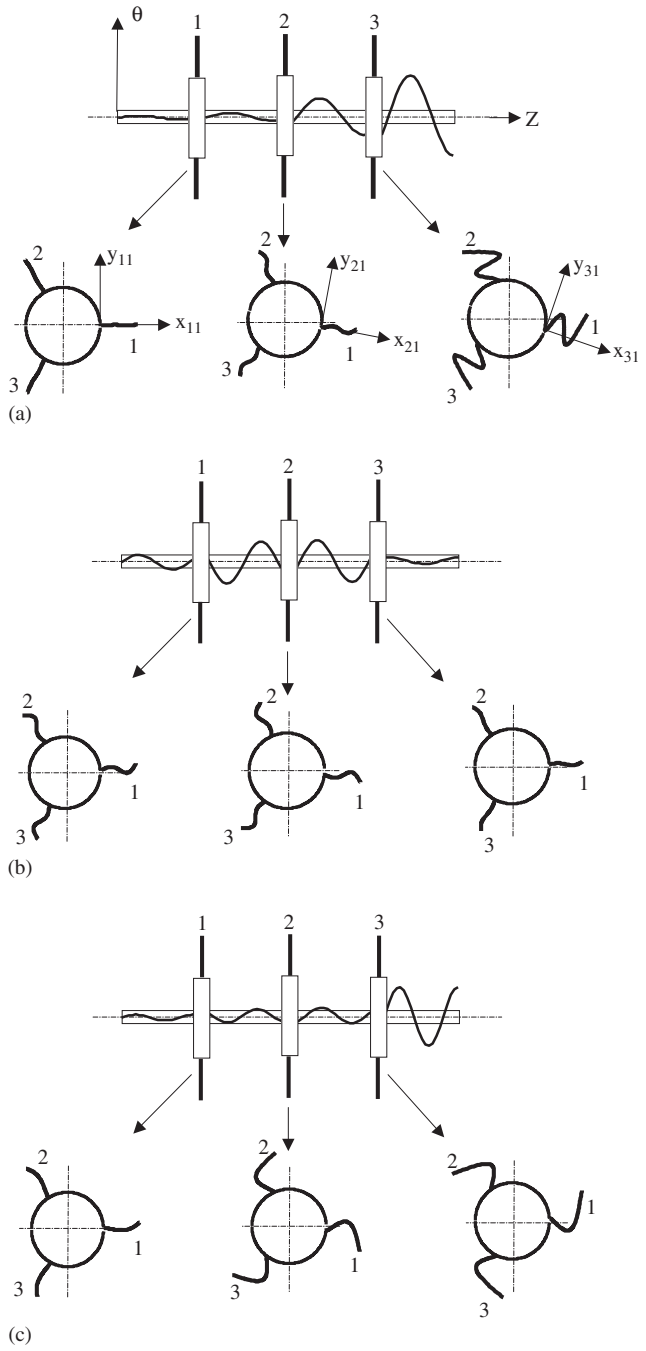

Fig. 11. Coupled shaft-torsion-blade–bending modes: metamorphosis of a mode shape during eigenvalue loci veering: (a) point A, $\beta = 10$, $\sigma = 104.2698$; (b) point B, $\beta = 20$, $\sigma = 133.6422$; (c) point C, $\beta = 40$, $\sigma = 153.7841$ of Fig. 10b2.

5. Conclusions

Linearly coupled shaft-torsional and blade-bending vibrations of multi-stage rotor-blade systems are studied. A synthetical, multi-frame and mixed approach is introduced to derive a mathematical model for the system.

It is shown that for a rotor with each stage carrying identical (tuned) blades, the eigenanalysis problem splits into two separate sub-problems each corresponding to a different kind of normal mode motion of the system. These are referred to as rigid shaft modes and coupled shaft-torsion–blade-bending modes by the authors. The coupled shaft-torsion–blade-bending modes are shown to exist in both single and multi-blade systems, while the rigid shaft modes are peculiar to multi-blade ones. The rigid shaft modes are such that the motions of the blades are in mutual balance and the shaft behaves like a rigid body. Therefore, the eigenanalysis related to these modes may be carried out separately on a rigid shaft-flexible blades model. The coupled shaft-torsion–blade-bending modes are shown to be subject to eigenvalue loci veering phenomena. This makes it necessary the coupling to be considered in the eigenanalysis whenever accuracy is required in the calculations.

The dimensions of the sub-problems replacing the main problem are independent of the number of blades. This amounts to a considerable model reduction for systems with high number of blades making thus possible systems with high number of stages to be treated without difficulty.

Before closing, a few remarks on some limitations of the presented analysis will be in order. First, the blades are modelled as uniform Euler–Bernouilli beams in this study. This abstraction made it possible to highlight the special features of the coupling between shaft torsional and blade in-plane bending vibrations. It should, however, be noted that in real bladings, the in-plane vibrations of the blades also couple with their torsional and out-of-plane vibrations, which, in turn, couple with the bending vibrations of the shaft. A more realistic model should, therefore, consider at least a quintuple coupling between shaft and blade vibrations. Another simplifying assumption was that about the identity of the blades of a same disk (tuned blades assumption). Important problems such as vibration localization in mistuned blades are, therefore, left beyond the scope of the study. As a final remark let it also be noted that along with the linear coupling treated in this study, nonlinear coupling also exists between shaft-torsional and blade-bending vibrations. Further analytical work is, therefore, required to thoroughly elucidate the coupling effects between shaft-torsional and blade-bending vibrations of rotor-blade systems.

Acknowledgement

This work was supported by ITU Research Found under grant No. BAP.11-05-52.

Appendix A

Details on the construction of global mass and stiffness matrices in the finite element modelling of torsional (or longitudinal) vibrations of prismatic bars can be found in many textbooks (see for example Ref. [23]). The non-dimensional parts of these matrices, corresponding to quadratic interpolation function, internal node placed at the middle of each element, consistent mass matrix, bar with left end fixed and element number n (matrix dimensions: $2n \times 2n$), are reproduced below for completeness.

$$\mathbf{K} = \frac{n}{3} \cdot \begin{bmatrix} 16 & -8 & & & & & & \\ -8 & 14 & -8 & 1 & & & \mathbf{0} & \\ & -8 & 16 & -8 & & & & \\ & 1 & -8 & 14 & -8 & 1 & & \\ & & & & \ddots & & & \\ & & & 1 & -8 & 14 & -8 & 1 \\ & \mathbf{0} & & & & -8 & 16 & -8 \\ & & & & & 1 & -8 & 7 \end{bmatrix}, \tag{A.1}$$

$$\mathbf{M} = \frac{1}{30 \cdot n} \cdot \begin{bmatrix} 16 & 2 & & & & & & \\ 2 & 8 & 2 & -1 & & & \mathbf{0} & \\ & 2 & 16 & 2 & & & & \\ & -1 & 2 & 8 & 2 & -1 & & \\ & & & & \ddots & & & \\ & & & -1 & 2 & 8 & 2 & -1 \\ & \mathbf{0} & & & & 2 & 16 & 2 \\ & & & & & -1 & 2 & 4 \end{bmatrix}. \tag{A.2}$$

Appendix B

The equation of motion of an Euler–Bernoilli beam subjected to a distributed force and a tip force will be derived. That equation can conveniently be used as a starting point in the vibration and stability analyses of beams undergoing overall motions.

Recall from elementary strength of materials that for small lateral displacements, the bending moment at a station x of a beam can be written as

$$M(x,t) = \mathrm{EI}\frac{\partial^2 y(x,t)}{\partial x^2}. \tag{B.1}$$

Then consider Fig. B1 depicting an Euler–Bernouilli beam of flexural rigidity EI, cross-sectional area A, mass density ρ and length ℓ, acted upon by a distributed force with components $f_x(x,t)$ and $f_y(x,t)$, a tip force with components $F_x(t)$ and $F_y(t)$, and also by the distributed inertia force

$$F_{\mathrm{in}}(x,t) = -\rho A\frac{\partial^2 y(x,t)}{\partial t^2}. \tag{B.2}$$

In view of this figure $M(x,t)$ can be expressed as

$$\begin{aligned} M(x,t) = & -F_x(t)\cdot\left[\int_x^\ell \frac{\partial y(\eta,t)}{\partial \eta}\,\mathrm{d}\eta\right] - \int_x^\ell \left\{ f_x(\xi,t)\cdot\left[\int_x^\xi \frac{\partial y(\eta,t)}{\partial \eta}\,\mathrm{d}\eta\right]\right\}\cdot \mathrm{d}\xi \\ & + F_y(t)\cdot\int_x^\ell \mathrm{d}\eta + \int_x^\ell \left\{\left[f_y(\xi,t) - \rho A\frac{\partial^2 y(\xi,t)}{\partial t^2}\right]\cdot\left(\int_x^\xi \mathrm{d}\eta\right)\right\}\cdot \mathrm{d}\xi, \end{aligned} \tag{B.3}$$

where ξ and η are dummy variables standing for x, and the integrals with respect to η represent the moment arms of the related forces. Now, insert Eq. (B.3) into Eq. (B.1), take the second partial derivative with respect

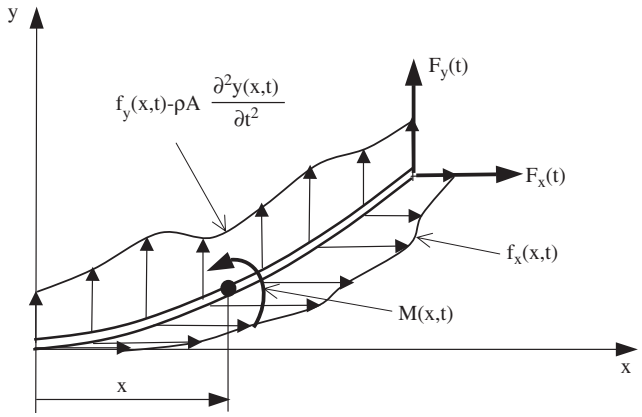

Fig. B1. Beam subjected to distributed and tip forces.

to x by using the Leibniz rule and obtain

$$\rho A\frac{\partial^2 y(x,t)}{\partial t^2}+\mathrm{EI}\frac{\partial^4 y(x,t)}{\partial x^4}-\left[F_x(t)+\int_x^\ell f_x(\xi,t)\,\mathrm{d}\xi\right]\frac{\partial^2 y(x,t)}{\partial x^2}+f_x(x,t)\frac{\partial y(x,t)}{\partial x}-f_y(x,t)=0 \tag{B.4}$$

as the integro-partial differential equation of motion of an Euler–Bernouilli beam subjected to a distributed force and a tip force. (See Ref. [24, p. 326] for a similar equation given in a slightly different context.) Setting the tip force component $F_x(t)$ to zero one obtains Eq. (3) above.

It should be noticed that, in this formulation, the tip force component $F_y(t)$ does not appear in the equation of motion. It is to be accounted for in the boundary conditions.

Appendix C

The dimensionless natural frequencies of a stationary cantilever are the roots of the transandantal equation $1+\cos\lambda\cosh\lambda=0$. The first five of them are calculated to be $\lambda_1=1.87510407$, $\lambda_2=4.69409113$, $\lambda_3=7.85475744$, $\lambda_4=10.99554073$, $\lambda_5=14.13716839$. Thus, according to Eq. (14) one has for $m=5$

$$\mathbf{A}=\begin{bmatrix} -1.57087819 & & & & \\ 0.42232039 & -8.64714269 & & \text{symmetric} & \\ 1.07208483 & -1.89005471 & -24.95211331 & & \\ 0.87313772 & 3.64338461 & -8.33828978 & -51.45910508 & \\ 0.76232572 & 3.06280535 & 7.14108671 & -19.01912840 & -87.79232739 \end{bmatrix}, \tag{C.1}$$

$$\mathbf{B}=\begin{bmatrix} -1.19333637 & & & & \\ 0.68585528 & -6.47822486 & & \text{symmetric} & \\ 0.79237922 & -0.16940788 & -17.85951988 & & \\ 0.54641327 & 2.91185111 & -3.27427206 & -36.05538833 & \\ 0.45407544 & 1.88916672 & 6.15441659 & -8.57015737 & -60.80107624 \end{bmatrix}, \tag{C.2}$$

$$\mathbf{c}=\begin{Bmatrix} 0.78299176 & 0.4339359 & 0.2544253 & 0.18189802 & 0.14147084 \end{Bmatrix}^{\mathrm{T}}, \tag{C.3}$$

$$\mathbf{d}=\begin{Bmatrix} 0.56882574 & 0.09076679 & 0.03241637 & 0.01654234 & 0.01000703 \end{Bmatrix}^{\mathrm{T}}. \tag{C.4}$$

Appendix D

Consider a certain ith hyper-row (related to the ith blade-carrying disk) of the eigenproblem of Eq. (22), note, in view of Eqs. (20) and (23), that it is formed of k_i sub-hyper-rows, each corresponding to one blade, take the difference of any two of these sub-hyper-rows (say the jth and the kth) to obtain

$$[\mathbf{K}_{ii}-\sigma^2\mathbf{I}]\{\mathbf{G}_{ij}-\mathbf{G}_{ik}\}=\{\mathbf{0}\};\quad i=1,2,\ldots,p. \tag{D.1}$$

Then, for any selection of i, either

$$\det[\mathbf{K}_{ii}-\sigma^2\mathbf{I}]=0 \tag{D.2}$$

or

$$\mathbf{G}_{ij}=\mathbf{G}_{ik}(=\mathbf{G}_i,\text{say}). \tag{D.3}$$

(i) Consider first the case where

$$\det[\mathbf{K}_{ii}-\sigma^2\mathbf{I}]\neq 0\quad \forall i=1,2,\ldots,p. \tag{D.4}$$

Then Eq. (D.3) holds true for all i's,

$$\mathbf{G}_{ij}=\mathbf{G}_{ik}=\mathbf{G}_i\quad \forall i=1,2,\ldots,p \tag{D.5}$$

and this renders all the sub-hyper-rows related to the ith disk identical. Taking one sub-hyper-row for each disk, Eq. (22) yields

$$\left[\begin{bmatrix} \mathbf{A}_{00} & k_1\delta_1\mathbf{B}_{01} & k_2\delta_2\mathbf{B}_{02} & \cdots & k_p\delta_p\mathbf{B}_{0p} \\ \mathbf{C}_{10} & \mathbf{K}_{11}+k_1\delta_1\mathbf{D}_{11} & k_2\delta_2\mathbf{D}_{12} & \cdots & k_p\delta_p\mathbf{D}_{1p} \\ \mathbf{C}_{20} & k_1\delta_1\mathbf{D}_{21} & \mathbf{K}_{22}+k_2\delta_2\mathbf{D}_{22} & \cdots & k_p\delta_p\mathbf{D}_{2p} \\ \vdots & \vdots & \vdots & \ddots & \vdots \\ \mathbf{C}_{p0} & k_1\delta_1\mathbf{D}_{p1} & k_2\delta_2\mathbf{D}_{p2} & \cdots & \mathbf{K}_{pp}+k_p\delta_p\mathbf{D}_{pp} \end{bmatrix} - \sigma^2\mathbf{I}\right] \begin{Bmatrix} \mathbf{\Theta} \\ \mathbf{G}_1 \\ \mathbf{G}_2 \\ \vdots \\ \mathbf{G}_p \end{Bmatrix} = \begin{Bmatrix} \mathbf{0} \\ \mathbf{0} \\ \mathbf{0} \\ \vdots \\ \mathbf{0} \end{Bmatrix}. \tag{D.6}$$

From Eqs. (D.5) and (D.6) follow Eqs. (27) and (30) defining the eigenanalysis sub-problem of coupled shaft-torsion–blade-bending modes.

(ii) Next consider the case where

$$\det\lfloor \mathbf{K}_{ii} - \sigma^2\mathbf{I}\rfloor = 0 \quad \text{for } i = r \tag{D.7}$$

and

$$\mathbf{G}_{ij} = \mathbf{G}_{ik} = \mathbf{G}_i \quad \text{for} \quad i \neq r. \tag{D.8}$$

In this case, to any sth eigenvalue σ_s of Eq. (D.7) with $i = r$ there corresponds an eigenvector $\mathbf{U}_r^{(s)} = \{\mathbf{G}_{rj} - \mathbf{G}_{rk}\}^{(s)}$ of Eq. (D.1). Noting that this eigenvector is independent of the choice of j and k, one concludes that all the vectors $\mathbf{G}_{rj}$ must have the same form as $\mathbf{U}_r^{(s)}$ in the sth mode. Thus one may write

$$\mathbf{G}_r^{(s)} = \mathbf{U}_r^{(s)}, \quad \mathbf{G}_{rj}^{(s)} = \alpha_{rj}^{(s)} \cdot \mathbf{G}_r^{(s)}, \quad \forall j, s, \tag{D.9}$$

where $\alpha_{rj}^{(s)}$ is a constant scaling factor. In view of Eqs. (D.7)–(D.9), Eq. (22) gives

$$\begin{bmatrix} \mathbf{A}_{00}-\sigma_s^2\mathbf{I} & k_1\delta_1\mathbf{B}_{01} & \cdots & a_r^{(s)}\delta_r\mathbf{B}_{01} & \cdots & k_p\delta_p\mathbf{B}_{0p} \\ \mathbf{C}_{10} & \mathbf{K}_{11}+k_1\delta_1\mathbf{D}_{11}-\sigma_s^2\mathbf{I} & \cdots & a_r^{(s)}\delta_r\mathbf{D}_{1r} & \cdots & k_p\delta_p\mathbf{D}_{1p} \\ \vdots & \vdots & \vdots & \vdots & \vdots & \vdots \\ \mathbf{C}_{r0} & k_1\delta_1\mathbf{D}_{r1} & \cdots & a_r^{(s)}\delta_r\mathbf{D}_{rr} & \cdots & k_p\delta_p\mathbf{D}_{rp} \\ \vdots & \vdots & \vdots & \vdots & \vdots & \vdots \\ \mathbf{C}_{p0} & k_1\delta_1\mathbf{D}_{p1} & \cdots & a_r^{(s)}\delta_r\mathbf{D}_{rr} & \cdots & \mathbf{K}_{pp}+k_p\delta_p\mathbf{D}_{pp}-\sigma_s^2\mathbf{I} \end{bmatrix} \begin{Bmatrix} \mathbf{\Theta}^{(s)} \\ \mathbf{G}_1^{(s)} \\ \vdots \\ \mathbf{G}_r^{(s)} \\ \vdots \\ \mathbf{G}_p^{(s)} \end{Bmatrix} = \begin{Bmatrix} \mathbf{0} \\ \mathbf{0} \\ \vdots \\ \mathbf{0} \\ \vdots \\ \mathbf{0} \end{Bmatrix}, \tag{D.10}$$

where

$$a_r^{(s)} = \sum_{j=1}^{k_r} \alpha_{rj}^{(s)}. \tag{D.11}$$

In Eq. (D.10) $\mathbf{G}_r^{(s)}$ is known from Eq. (D.9) while $a_r^{(s)}$ is unknown. It is convenient to rearrange that equation so as to put all the unknowns together,

$$\begin{bmatrix} \mathbf{A}_{00}-\sigma_s^2\mathbf{I} & k_1\delta_1\mathbf{B}_{01} & \cdots & \delta_r\mathbf{B}_{01}\mathbf{G}_r^{(s)} & \cdots & k_p\delta_p\mathbf{B}_{0p} \\ \mathbf{C}_{10} & \mathbf{K}_{11}+k_1\delta_1\mathbf{D}_{11}-\sigma_s^2\mathbf{I} & \cdots & \delta_r\mathbf{D}_{1r}\mathbf{G}_r^{(s)} & \cdots & k_p\delta_p\mathbf{D}_{1p} \\ \vdots & \vdots & \vdots & \vdots & \vdots & \vdots \\ \mathbf{C}_{r0} & k_1\delta_1\mathbf{D}_{r1} & \cdots & \delta_r\mathbf{D}_{rr}\mathbf{G}_r^{(s)} & \cdots & k_p\delta_p\mathbf{D}_{rp} \\ \vdots & \vdots & \vdots & \vdots & \vdots & \vdots \\ \mathbf{C}_{p0} & k_1\delta_1\mathbf{D}_{p1} & \cdots & \delta_r\mathbf{D}_{rr}\mathbf{G}_r^{(s)} & \cdots & \mathbf{K}_{pp}+k_p\delta_p\mathbf{D}_{pp}-\sigma_s^2\mathbf{I} \end{bmatrix} \begin{Bmatrix} \mathbf{\Theta}^{(s)} \\ \mathbf{G}_1^{(s)} \\ \vdots \\ a_r^{(s)} \\ \vdots \\ \mathbf{G}_p^{(s)} \end{Bmatrix} = \begin{Bmatrix} \mathbf{0} \\ \mathbf{0} \\ \vdots \\ \mathbf{0} \\ \vdots \\ \mathbf{0} \end{Bmatrix}. \tag{D.12}$$

Thus, either the determinant of the coefficients' matrix of Eq. (D.12) is zero (which is in general not the case because all the elements of the matrix are independently given quantities), or it has only trivial solution (which is deduced to be the case here). Whence, one is led to the results summarized in Eqs. (31) and (32).

On the other hand, returning to Eq. (22) and performing a series of elementary matrix operations on its coefficients' matrix one is led to the characteristic equation

$$\det\left[\begin{array}{c|c} \mathbf{X} & \mathbf{Y} \\ \hline \mathbf{0} & \mathbf{Z} \end{array}\right] = 0, \tag{D.13}$$

where $\mathbf{0}$ is the zero matrix and

$$\mathbf{X} = \begin{bmatrix} \mathbf{A}_{00} - \sigma^2\mathbf{I} & k_1\delta_1\mathbf{B}_{01} & k_2\delta_2\mathbf{B}_{02} & \cdots & k_p\delta_p\mathbf{B}_{0p} \\ k_1\mathbf{C}_{10} & \mathbf{K}_{11} + k_1\delta_1\mathbf{D}_{11} - \sigma^2\mathbf{I} & k_2\delta_2\mathbf{D}_{12} & \cdots & k_p\delta_p\mathbf{D}_{1p} \\ k_2\mathbf{C}_{20} & k_1\delta_1\mathbf{D}_{21} & \mathbf{K}_{22} + k_2\delta_2\mathbf{D}_{22} - \sigma^2\mathbf{I} & \cdots & k_p\delta_p\mathbf{D}_{2p} \\ \vdots & \vdots & \vdots & \ddots & \vdots \\ k_p\mathbf{C}_{p0} & k_1\delta_1\mathbf{D}_{p1} & k_2\delta_2\mathbf{D}_{p2} & \cdots & \mathbf{K}_{pp} + k_p\delta_p\mathbf{D}_{pp} - \sigma^2\mathbf{I} \end{bmatrix}, \tag{D.14}$$

$$\mathbf{Z} = \begin{bmatrix} \mathbf{Z}_{11} & \mathbf{0} & \cdots & \mathbf{0} \\ \mathbf{0} & \mathbf{Z}_{22} & \cdots & \mathbf{0} \\ \vdots & \vdots & \ddots & \vdots \\ \mathbf{0} & \mathbf{0} & \cdots & \mathbf{Z}_{pp} \end{bmatrix}, \tag{D.15}$$

where $\mathbf{Z}_{ii}$'s are block diagonal matrices with k_i-1 identical blocks

$$\mathbf{Z}_{ii} = \begin{bmatrix} \mathbf{K}_{ii} - \sigma^2\mathbf{I} & \mathbf{0} & \cdots & \mathbf{0} \\ \mathbf{0} & \mathbf{K}_{ii} - \sigma^2\mathbf{I} & \cdots & \mathbf{0} \\ \vdots & \vdots & \ddots & \vdots \\ \mathbf{0} & \mathbf{0} & \cdots & \mathbf{K}_{ii} - \sigma^2\mathbf{I} \end{bmatrix}, \tag{D.16}$$

with the matrices $\mathbf{K}_{ii}$ as given in Eq. (21). (It may also be of interest to note here that the "1" in the number k_i-1 is eventually a result of the fact that only "one" degree-of-freedom of the shaft couples with the blades of a given disk in the considered model.) From Eqs. (D.13)–(D.16) follows the characteristic equation, Eq. (25) of the system. Note that this result is also in accordance with Eqs. (D.6) and (D.7).

The results obtained here are also in agreement with those obtained by Ren et al. [25] for systems with a single disk carrying a number of tuned blades.

References

[1] A.V. Srinivasan, Flutter and resonant vibration characteristics of engine blades, *Journal of Engineering for Gas Turbines and Power* 119 (1997) 743–775.

[2] D.J. Ewins, Vibration characteristics of bladed disc assemblies, *Journal of Mechanical Engineering Science* 15 (3) (1973) 165–186.

[3] R. Bladh, C. Pierre, M.P. Castanier, M.J. Kruse, Dynamic response predictions for a mistuned industrial turbomachinery rotor using reduced-order modelling, *Journal of Engineering for Gas Turbines and Power* 124 (2002) 311–324.

[4] G.C. Tsai, Rotating vibration behavior of turbine blades with different groups of blades, *Journal of Sound and Vibration* 271 (2004) 547–575.

[5] R.G. Loewy, N. Khader, Structural dynamics of rotating bladed-disk assemblies coupled with flexible shaft motions, *AIAA Journal* 22 (9) (1984) 1319–1327.

[6] E.F. Crawley, E.H. Ducharme, D.R. Mokadam, Analytical and experimental investigation of the coupled bladed disk/shaft whirl of a cantilevered turbofan, *Journal of Engineering for Gas Turbines and Power* 108 (1986) 567–576.

[7] S.B. Chun, C.W. Lee, Vibration analysis of shaft-bladed disk system by using substructure synthesis and assumed modes method, *Journal of Sound and Vibration* 189 (5) (1996) 587–608.

[8] A. Okabe, et al., An equivalent reduced modelling method and its application to shaft-blade coupled torsional vibration analysis of a turbine-generator set, *Journal of Power and Energy* 205 (1991) 173–181.
[9] S.C. Huang, K.B. Ho, Coupled shaft-torsion and blade-bending vibrations of a rotating shaft-disk-blade unit, *Journal of Engineering for Gas Turbines and Power* 118 (1996) 100–106.
[10] E. Chatelet, F. D'Ambrosio, G. Jacquet-Richardet, Toward global modelling approaches for dynamic analyses of rotating assemblies of turbomachines, *Journal of Sound and Vibration* 282 (2005) 163–178.
[11] R.V. Southwell, F. Gaugh, The free transverse vibration of airscrew blades, British A.R.C. Report and Memoranda No. 766, 1921.
[12] D.A. Peters, An approximate solution for the free vibrations of rotating uniform cantilever beams, NASA TMX-62, 299, 1973.
[13] C.H.J. Fox, J.S. Burdess, The natural frequencies of a thin rotating cantilever with offset root, *Journal of Sound and Vibration* 65 (2) (1979) 151–158.
[14] A.D. Wright, C.E. Smith, R.W. Tresher, J.L.C. Wang, Vibration modes of centrifugally stiffened beams, *Journal of Applied Mechanics* 49 (1982) 197–202.
[15] S. Naguleswaran, Lateral vibration of a centrifugally tensioned uniform Euler–Bernouilli beam, *Journal of Sound and Vibration* 176 (5) (1994) 613–624.
[16] Y.N. Al-Nassar, B.O. Al-Bedoor, On the vibration of a rotating blade on a torsionally flexible shaft, *Journal of Sound and Vibration* 259 (5) (2003) 1237–1242.
[17] Ö. Turhan, G. Bulut, Dynamic stability of rotating blades (beams) eccentrically clamped to a shaft with fluctuating speed, *Journal of Sound and Vibration* 280 (2005) 945–964.
[18] F.R. Gantmacher, *Théorie des matrices, Tome 1: Théorie générale*, Dunod, Paris, 1966.
[19] H. Lütkepohl, *Handbook of Matrices*, Wiley, New York, 1996.
[20] Y.G. Jei, C.W. Lee, Does curve veering occur in the eigenvalue problem of rotors?, *Journal of Vibration and Acoustics* 114 (1992) 32–36.
[21] N. Mostaghel, I. Tadjbakhsh, Buckling of rotating rods and plates, *International Journal of Mechanical Sciences* 15 (1973) 429–434.
[22] D.A. Peters, D.H. Hodges, In-plane vibration and buckling of a rotating beam clamped off the axis of rotation, *Journal of Applied Mechanics* 47 (1980) 398–402.
[23] L. Meirovitch, *Elements of Vibration Analysis*, second ed., McGraw-Hill, New York, 1986.
[24] H. Leipholz, *Stability of Elastic Systems*, Sijthoff & Noordhoff, Alphan a/d Rijn, 1986.
[25] G.X. Ren, Z.C. Zheng, W.J. Wang, Vibration characteristics of systems with multiple blades, *Journal of Sound and Vibration* 225 (4) (1999) 597–610.